Journal of Scientific Computing (2024) 101:21
https://doi.org/10.1007/s10915-024-02665-4

# A Modified Interior Penalty Virtual Element Method for Fourth-Order Singular Perturbation Problems

**Fang Feng**[1] · **Yue Yu**[2]

Received: 17 December 2023 / Revised: 22 August 2024 / Accepted: 24 August 2024 /
Published online: 4 September 2024


**Abstract**
This paper is dedicated to the numerical solution of a fourth-order singular perturbation problem using the interior penalty virtual element method (IPVEM). Compared with the original IPVEM proposed in Zhao et al. (Math Comp 92(342):1543–1574, 2023), the study introduces modifications to the jumps and averages in the penalty term, as well as presents a mesh-dependent selection of the penalty parameter. Drawing inspiration from the modified Morley finite element methods, we leverage the conforming interpolation technique to handle the lower part of the bilinear form in the error analysis. We establish the optimal convergence in the energy norm and provide a rigorous proof of uniform convergence concerning the perturbation parameter in the lowest-order case.

**Keywords** Interior penalty virtual element method · Fourth-order singular perturbation problem · Uniform error estimates · Perturbation parameter · Modified Morley element

## 1 Introduction

Let $\Omega$ be a bounded polygonal domain of $\mathbb{R}^2$ with boundary $\partial\Omega$. For $f \in L^2(\Omega)$, we consider the following boundary value problem of the fourth-order singular perturbation equation:

$$\begin{cases} \varepsilon^2 \Delta^2 u - \Delta u = f \ \text{ in } \ \Omega, \\ u = \dfrac{\partial u}{\partial \boldsymbol{n}} = 0 \qquad \text{on } \ \partial\Omega, \end{cases} \tag{1.1}$$

where $\boldsymbol{n} = (n_1, n_2)$ is the unit outer normal to $\partial\Omega$, $\Delta$ is the standard Laplacian operator and $\varepsilon$ is a real parameter satisfying $0 < \varepsilon \leq 1$. This equation can be considered as a linear model for

✉ Yue Yu
terenceyuyue@xtu.edu.cn

Fang Feng
ffeng@njust.edu.cn

[1] School of Mathematics and Statistics, Nanjing University of Science and Technology, Nanjing 210094, Jiangsu, People's Republic of China

[2] Hunan Key Laboratory for Computation and Simulation in Science and Engineering, Key Laboratory of Intelligent Computing and Information Processing of Ministry of Education, National Center for Applied Mathematics in Hunan, School of Mathematics and Computational Science, Xiangtan University, Xiangtan 411105, Hunan, People's Republic of China

a clamped thin elastic plate under tension that is subjected to a transverse loading (represented by the function $f$), with $\varepsilon$ quantifying the ratio of bending rigidity to tensile stiffness in the plate. As $\varepsilon$ approaches zero, this plate model degenerates into an elastic membrane problem. Such problems also arise when studying the linearization of the vanishing moment method for the fully nonlinear Monge-Ampère equation [13, 35, 44].

When $\varepsilon$ is not small, the problem can be numerically resolved as the biharmonic equation by using some standard finite element methods for fourth-order problems. However, in this article, we are primarily concerned with the case where $\varepsilon \to 0$, or the differential equation formally degenerates to the Poisson equation (see (4.14)), but with the "extra" normal boundary condition in (1.1), which will produce boundary layers in the first derivatives of $u$ [35]. Due to the presence of the fourth-order term, $H^2$-conforming finite elements with $C^1$ continuity were considered in [35], but these methods are quite complicated even in two dimensions. To overcome this difficulty, it is preferred to use nonconforming finite elements. Since the differential equation reduces to the Poisson equation in the singular limit, $C^0$-conforming finite elements are better suited for the task, as shown in [33]. In that work, the method was proved to converge uniformly in the perturbation parameter in the energy norm, and a counterexample was given to show that the Morley method diverges for the reduced second-order equation (see also the patch test in [40]). Considering that the Morley element has the least number of element degrees of freedom (DoFs), Wang et al. proposed in [41] a modified Morley element method. This method still uses the DoFs of the Morley element, but linear approximation of finite element functions is used in the lower part of the bilinear form:

$$\varepsilon^2 a_h(u_h, v_h) + b_h(\Pi_h^1 u_h, \Pi_h^1 v_h) = (f, \Pi_h^1 v_h), \tag{1.2}$$

where

$$a_h(v_h, w_h) = \sum_{K \in \mathcal{T}_h} (\nabla^2 v_h, \nabla^2 w_h)_K, \qquad b_h(v_h, w_h) = \sum_{K \in \mathcal{T}_h} (\nabla v_h, \nabla w_h)_K,$$

and $\Pi_h^1$ is the interpolation operator corresponding to linear conforming element for second-order partial differential equations. It was also shown that the modified method converges uniformly in the perturbation parameter. On the other hand, among the robust methods with respect to the singular parameter $\varepsilon$, the $C^0$ interior penalty methods [13, 15] may be most attractive as they utilize the standard $C^0$ finite element spaces. These spaces are primarily designed for solving second-order problems and effectively reduce the computational cost to a certain extent.

This paper focuses on virtual element methods (VEMs), which are a generalization of the standard finite element method that allows for general polytopal meshes. First proposed and analyzed in [7], with other pioneering works found in [2, 8], VEMs have several advantages over standard finite element methods. For example, they are more convenient for handling partial differential equations on complex geometric domains or those associated with high-regularity admissible spaces. To date, a considerable number of conforming and nonconforming VEMs have been developed to address second-order elliptic equations [2, 7, 20, 26] as well as fourth-order elliptic equations [6, 17, 22, 24, 48]. The versatility and effectiveness of the VEM have made it a popular choice for tackling a wide range of scientific and engineering problems, including the Stokes problem [5, 19, 32], the Navier–Stokes equation [10, 11, 29], the magnetohydrodynamic system [3, 9], the sine-Gordon equation [1], the topology optimization problems [5, 23, 46], the fourth-order singular perturbation problems [45] and the variational and hemivariational inequalities [27, 28, 31, 34, 37–39,

43]. For a comprehensive understanding of recent advancements in the VEM, we recommend referring to the book [4] and the associated references.

Recently, the interior penalty technique for VEMs has been explored in [47] for the biharmonic equation, which is equipped with the same DoFs for the $H^1$-conforming virtual elements [7], and the numerical scheme can be regarded as a combination of the virtual element space and discontinuous Galerkin scheme, since the resulting global discrete space is not $C^0$-continuous and an interior penalty formulation is adopted to enforce the continuity of the solution. The interior penalty method is then applied to address the fourth-order singular perturbation problem in [44], with some adaptations to the original space. These modifications encompass alterations in the definition of the $H^1$-type projection and the selection of the DoFs. Compared to the $C^0$-continuous nonconforming virtual element method in [45], the IPVEM boasts a reduced number of the DoFs, rendering it more appropriate for tackling fourth-order singular perturbation problems.

In contrast to the methodology in [44], we adopt the original formulation introduced in [47] to address the fourth-order singular perturbation problem (1.1). However, since the original IPVEM space lacks $C^0$ continuity, it brings some troubles on the error analysis for the consistency error for the lower part of the bilinear form as for the method in [44]. Specifically, when $u$ denotes the exact solution to (1.1) and $v_h$ represents a function in the original IPVEM space $V_h$, we encounter the consistency term

$$\sum_{e\in\mathcal{E}_h}\int_e \frac{\partial u}{\partial \boldsymbol{n}_e}[v_h]\mathrm{d}s, \qquad v_h \in V_h,$$

with $\mathcal{E}_h$ denoting the set of edges in the subdivision and $[v_h]$ the jump across $e$. In the error analysis, it is expected that this consistency term either vanishes or exhibits an error on the order of $\mathcal{O}(h^\alpha)$ for some $\alpha \geq 1$. The comparison of the treatments for this consistency term is summarized as follows.

- For the method in [44], the authors developed a new space with new DoFs by using a revised projection to impose some restrictions on the local space of $H^2$-conforming virtual element. This adjustment ensures the continuity of the moments of functions on edges in the lowest-order case, i.e., $\int_e [v_h]\mathrm{d}s = 0$ or $\Pi^0_{0,e}[v_h] = 0$ (in the lowest order case), where $\Pi^0_{0,e}$ represents the $L^2$ projector onto $\mathbb{P}_0(e)$, leading to (see Eq. (4.27) in [44]):

$$\begin{aligned}\sum_{e\in\mathcal{E}_h}\int_e \frac{\partial u}{\partial \boldsymbol{n}_e}[v_h]\mathrm{d}s &= \sum_{e\in\mathcal{E}_h}\int_e \frac{\partial u}{\partial \boldsymbol{n}_e}([v_h]-\Pi^0_{0,e}[v_h])\mathrm{d}s\\ &\leq \sum_{e\in\mathcal{E}_h}\left\|\frac{\partial u}{\partial \boldsymbol{n}_e}\right\|_{0,e}\|[v_h]-\Pi^0_{0,e}[v_h]\|_{0,e} \lesssim h|u|_2|v_h|_{1,h}.\end{aligned}$$

  This nonconformity error is not optimal (see the remark below Theorem 4.5 of [44]), which was observed in the numerical test with a higher convergence rate as $\varepsilon$ becomes small.
- Inspired by the technique in (1.2) for discontinuous elements, we address this issue by introducing a linear conforming interpolation operator in the lower part of the bilinear form. Consequently, the consistency term can be expressed as

$$\sum_{e\in\mathcal{E}_h}\int_e \frac{\partial u}{\partial \boldsymbol{n}_e}[I_h^c v_h]\mathrm{d}s, \qquad v_h \in V_h,$$

where $I_h^c$ is the conforming interpolation operator for $V_h$. Since $I_h^c v_h$ is continuous across the edges, the above term naturally vanishes, a departure from the concept of enforcing weak continuity of $v_h$ along edges as discussed in [44]. In this case, we get the optimal estimate for the nonconformity error as shown in Theorem 4.1. It is worth noting that in the context of VEMs, the linear conforming interpolation operator can be omitted as it yields the same first-order elliptic projection (see Remark 3.2). For this reason, there is no need to modify the lower part, and the modification is solely utilized in the error analysis. From this point of view, the original interior penalty virtual elements exhibit similar behaviors to $C^0$-continuous elements despite its discontinuity.

The remainder of the paper is structured as follows. We begin by introducing the continuous variational problem and presenting some useful results in VEM analysis in Sect. 2. Section 3 is dedicated to the introduction of the IPVEM. In contrast to the jump and average terms in [47], we include the elliptic projector $\Pi_h^\nabla$ for all $v$ and $w$ in the penalty terms $J_i(v, w)$ for $i = 1, 2, 3$ to simplify the implementation. This modification can be interpreted by the numerical integration (see Remark 3.1). Consequently, the resulting approach is denoted as a modified IPVEM (mIPVEM). Additionally, we provide a heuristic mesh-dependent selection of the penalty parameter $\lambda_e$, following a similar deduction as described in [18]. In Sect. 4, we establish the optimal convergence of the mIPVEM in the energy norm and provide a uniform error estimate in the lowest-order case. Our analysis demonstrates that the mIPVEM is robust with respect to the perturbation parameter. This is based on the observation that we can equivalently include the $H^1$-conforming interpolation in the lower part of the bilinear form, as in (1.2), since all required degrees of freedom are accessible. Numerical examples for second- and third-order virtual elements are presented in Sect. 5 to validate the theoretical predictions.

## 2 The Continuous Variational Problem

We first introduce some notations and symbols frequently used in this paper. For a bounded Lipschitz domain $D$ of dimension $d$ ($d = 1, 2$), the symbol $(v, w)_D = \int_D vw\mathrm{d}x$ denotes the $L^2$-inner product on $D$, $\|\cdot\|_{0,D}$ or $\|\cdot\|_D$ denotes the $L^2$-norm, and $|\cdot|_{s,D}$ is the $H^s(D)$-seminorm. If $D = \Omega$, for simplicity, we abbreviate $\|\cdot\|_\Omega$ as $\|\cdot\|$. For vectorial functions $\boldsymbol{v} = (v_1, v_2)^T$ and $\boldsymbol{w} = (w_1, w_2)^T$, the inner product is defined as $(\boldsymbol{v}, \boldsymbol{w})_D = \int_D (v_1 w_1 + v_2 w_2)\mathrm{d}x$. For all integer $k \geq 0$, $\mathbb{P}_k(D)$ is the set of polynomials of degree $\leq k$ on $D$. The set of scaled monomials $\mathbb{M}_r(D)$ is given by

$$\mathbb{M}_r(D) := \left\{ \left( \frac{\boldsymbol{x} - \boldsymbol{x}_D}{h_D} \right)^{\boldsymbol{s}}, \quad |\boldsymbol{s}| \leq r \right\},$$

with the element denoted by $m_D$, where $h_D$ is the diameter of $D$, $\boldsymbol{x}_D$ is the centroid of $D$, and $r$ is a non-negative integer. For the multi-index $\boldsymbol{s} \in \mathbb{N}^d$, we follow the usual notation

$$\boldsymbol{x}^{\boldsymbol{s}} = x_1^{s_1} \cdots x_d^{s_d}, \quad |\boldsymbol{s}| = s_1 + \cdots + s_d.$$

Conventionally, $\mathbb{M}_r(D) = \{0\}$ for $r \leq -1$.

Let $\mathcal{T}_h := \{K\}_{K \in \mathcal{T}_h}$ be a mesh of $\Omega$ into polygons. For a generic element $K$, define $h = \max_{K \in \mathcal{T}_h} h_K$ and $h_K = \mathrm{diam}(K)$. Let $e \subset \partial K$ be the common edge for elements $K = K_-$ and $K_+$, and let $v$ be a scalar function defined on $e$. We introduce the jump and average of $v$ on $e$ by $[v] = v^- - v^+$ and $\{v\} = \frac{1}{2}(v^- + v^+)$, where $v^-$ and $v^+$ are the traces of $v$ on $e$ from the interior and exterior of $K$, respectively. On a boundary edge, $[v] = v$ and

$\{v\} = v$. Moreover, for any two quantities $a$ and $b$, "$a \lesssim b$" indicates "$a \leq Cb$" with the constant $C$ independent of the mesh size $h_K$, and "$a \eqsim b$" abbreviates "$a \lesssim b \lesssim a$".

The variational formulation of (1.1) reads: Find $u \in V := H_0^2(\Omega)$ such that

$$\varepsilon^2 a(u, v) + b(u, v) = (f, v), \quad v \in H_0^2(\Omega), \tag{2.1}$$

where $a(u, v) = (\nabla^2 u, \nabla^2 v)$ and $b(u, v) = (\nabla u, \nabla v)$.

According to [33, Lemma 5.1], if $f \in L^2(\Omega)$ and $\Omega$ is a convex polygonal domain, then the weak solution $u \in H_0^2(\Omega) \cap H^3(\Omega)$, i.e., there exists a constant $c = c(\varepsilon)$ independent of $f$ such that $\|u\|_3 \leq c\|f\|_{-1}$, where $c$ depends on $\varepsilon$ and may blow up as $\varepsilon$ tends to zero (see Lemma 4.5). However, for general polygonal domains, the solution $u$ only belongs to $H^{2+\alpha}(\Omega)$ whenever $f \in H^{-2+\alpha}(\Omega)$ for some $\alpha \in (1/2, 1]$ [15]. In this article, we always assume that $\Omega$ is a bounded convex polygon. In this case, if $f$ has higher regularity, viz., $f \in H^{s-4}(\Omega)$ with $s \geq 3$, we may assume that $u \in H_0^2(\Omega) \cap H^s(\Omega)$.

In the context of geometric subdivisions, we consider a family of polygonal meshes $\{\mathcal{T}_h\}_{h>0}$ satisfying the following condition (cf. [16, 21]):

**H**. For each $K \in \mathcal{T}_h$, there exists a "virtual triangulation" $\mathcal{T}_K$ of $K$ such that $\mathcal{T}_K$ is uniformly shape regular and quasi-uniform. The corresponding mesh size of $\mathcal{T}_K$ is proportional to $h_K$. Each edge of $K$ is a side of a certain triangle in $\mathcal{T}_K$.

As shown in [21], this condition covers the usual geometric assumptions frequently used in the context of VEMs. Under this geometric assumption, we can establish some fundamental results in VEM analysis as used in [30].

According to the standard Dupont-Scott theory (cf. [14]), for all $v \in H^l(K)$ $(0 \leq l \leq k)$ there exists a certain $q \in \mathbb{P}_{l-1}(K)$ such that

$$|v - q|_{m,K} \lesssim h_K^{l-m} |v|_{l,K}, \quad m \leq l. \tag{2.2}$$

The following trace and Poincaré-Friedrichs inequalities are very useful for our forthcoming analysis [12, 14].

**Lemma 2.1** *For any $K \in \mathcal{T}_h$, there hold*

$$\|v\|_{0,\partial K} \lesssim \|v\|_{0,K}^{1/2} \|v\|_{1,K}^{1/2} \lesssim \|v\|_{0,K} + \|v\|_{0,K}^{1/2} |v|_{1,K}^{1/2}, \quad v \in H^1(K), \tag{2.3}$$

$$\|v\|_{0,\partial K} \lesssim h_K^{1/2} |v|_{1,K} + h_K^{-1/2} \|v\|_{0,K}, \quad v \in H^1(K), \tag{2.4}$$

$$h_K^{-1} \|v\|_{0,K} \lesssim |v|_{1,K} + h_K^{-1} \left| \int_{\partial K} v \mathrm{d}s \right|, \quad v \in H^1(K), \tag{2.5}$$

$$h_K^{-1} \|v\|_{0,K} \lesssim |v|_{1,K} + h_K^{-2} \left| \int_{K} v \mathrm{d}s \right|, \quad v \in H^1(K). \tag{2.6}$$

## 3 The Interior Penalty Virtual Element Method

### 3.1 The $H^1$-Projection in the Lifting Space

An interior penalty virtual element method (IPVEM) was proposed in [47]. In the construction, the authors first introduced a $C^1$-continuous virtual element space

$$\widetilde{V}_{k+2}(K) = \left\{ v \in H^2(K) : \Delta^2 v \in \mathbb{P}_k(K), v|_e \in \mathbb{P}_{k+2}(e), \partial_{\boldsymbol{n}} v|_e \in \mathbb{P}_{k+1}(e), \ \ e \subset \partial K \right\}, \quad k \geq 2,$$

which can be viewed as the lifting version of the standard $k$th order $C^1$-continuous virtual element space for fourth-order singular perturbation problems. This local space can be equipped with the following DoFs (cf. [17, 24]):

- $\tilde{\chi}^p$ : the values of $v$ at the vertices of $K$,

$$\tilde{\chi}_z^p(v) = v(z), \quad z\text{is a vertex of}K. \tag{3.1}$$

- $\tilde{\chi}^g$: the values of $h_z \nabla v$ at the vertices of $K$,

$$\tilde{\chi}_z^g(v) = h_z \nabla v(z), \quad z\text{is a vertex of}K, \tag{3.2}$$

  where $h_z$ is a characteristic length attached to each vertex $z$, for instance, the average of the diameters of the elements having $z$ as a vertex.
- $\tilde{\chi}^e$: the moments of $v$ on edges up to degree $k-2$,

$$\tilde{\chi}_e(v) = |e|^{-1}(m_e, v)_e, \quad m_e \in \mathbb{M}_{k-2}(e), \quad e \subset \partial K. \tag{3.3}$$

- $\tilde{\chi}^n$: the moments of $\partial_{\boldsymbol{n}_e} v$ on edges up to degree $k-1$,

$$\tilde{\chi}_e^n(v) = (m_e, \partial_{\boldsymbol{n}_e} v)_e, \quad m_e \in \mathbb{M}_{k-1}(e), \quad e \subset \partial K. \tag{3.4}$$

- $\tilde{\chi}^K$: the moments on element $K$ up to degree $k$,

$$\tilde{\chi}_K(v) = |K|^{-1}(m_K, v)_K, \quad m_K \in \mathbb{M}_k(K). \tag{3.5}$$

Given $v_h \in \widetilde{V}_{k+2}(K)$, the usual definition of the $H^1$-elliptic projection $\Pi_K^\nabla v_h \in \mathbb{P}_k(K)$ is described by the following equations:

$$\begin{cases} (\nabla \Pi_K^\nabla v_h, \nabla q)_K = (\nabla v_h, \nabla q)_K, \quad q \in \mathbb{P}_k(K), \\ \sum\limits_{z \in \mathcal{V}_K} \Pi_K^\nabla v_h(z) = \sum\limits_{z \in \mathcal{V}_K} v_h(z), \end{cases} \tag{3.6}$$

where $\mathcal{V}_K$ is the set of the vertices of $K$. This elliptic projection can be computed using the DoFs (3.1)–(3.5) by checking the right-hand side of the integration by parts formula:

$$(\nabla v_h, \nabla q)_K = -(v_h, \Delta q)_K + \sum_{e \subset \partial K} \int_e v_h \partial_{\boldsymbol{n}_e} q \, \mathrm{d}s.$$

However, the goal of the IPVEM is to make $\Pi_K^\nabla v_h$ computable by only using the DoFs of $H^1$-conforming virtual element spaces given by (cf. [2, 7])

$$V_h^{1,c}(K) := \{v \in H^1(K) : \Delta v|_K \in \mathbb{P}_{k-2}(K) \ \text{ in } \ K, \quad v|_{\partial K} \in \mathbb{B}_k(\partial K)\},$$

where

$$\mathbb{B}_k(\partial K) := \{v \in C(\partial K) : v|_e \in \mathbb{P}_k(e), \quad e \subset \partial K\},$$

and the corresponding global virtual element space is

$$V_h^{1,c} = \{v \in C(\overline{\Omega}) : v|_K \in V_h^{1,c}(K), \ K \in \mathcal{T}_h\} \cap H_0^1(\Omega).$$

To do so, Ref. [47] considered the approximation of the right-hand side by some numerical formula. In view of the $\mathbb{P}_k$ accuracy, namely $\Pi_K^\nabla v_h = v_h$ for $v_h \in \mathbb{P}_k(K)$, the modified $H^1$-projection is defined as

$$\begin{cases} (\nabla \Pi_K^\nabla v_h, \nabla q)_K = -(v_h, \Delta q)_K + \sum\limits_{e \subset \partial K} Q_{2k-1}^e (v_h \partial_{\boldsymbol{n}_e} q), \quad q \in \mathbb{P}_k(K), \\ \sum_{z \in \mathcal{V}_K} \Pi_K^\nabla v_h(z) = \sum_{z \in \mathcal{V}_K} v_h(z), \end{cases}$$

with

$$Q^e_{2k-1}v := |e|\sum_{i=0}^{k}\omega_i v(\boldsymbol{x}_i^e) \approx \int_e v(s)\mathrm{d}s,$$

where $(\omega_i, \boldsymbol{x}_i^e)$ are the $(k+1)$ Gauss-Lobatto quadrature weights and points with $\boldsymbol{x}_0^e$ and $\boldsymbol{x}_k^e$ being the endpoints of $e$. The piecewise $H^1$-projector $\Pi_h^\nabla$ is defined by setting $\Pi_h^\nabla|_K = \Pi_K^\nabla$ for all $K \in \mathcal{T}_h$. In this case, the DoFs $\{\tilde{\boldsymbol{\chi}}^p, \tilde{\boldsymbol{\chi}}^e\}$ on $e$ should be replaced by the $(k+1)$ Gauss-Lobatto points. Notice that when $v_h \in \mathbb{P}_k(K)$, the integrand of $\int_e v_h \partial_{\boldsymbol{n}_e} q\,\mathrm{d}s$ is a polynomial of order $2k-1$ on $e$, while the algebraic accuracy is exactly $2k-1$ for the $(k+1)$ Gauss-Lobatto points. In particular, we have $2k-1=3$ for $k=2$, corresponding to the Simpson's rule.

For the computation of the $L^2$ projector $\Pi^k_{0,K}$ onto $\mathbb{P}_k(K)$, we can decrease the degrees of freedom by employing the standard enhancement technique [2]. In fact, one can find that the moments on element $K$ with degrees $k-1$ and $k$ are not required for the computation of the modified $H^1$-elliptic projection. For this reason, we substitute the redundant moments of $v$ with those of $\Pi_K^\nabla v$. The resulting space is given by

$$W_k(K) := \{v \in H^2(K) : \Delta^2 v \in \mathbb{P}_{k-2}(K),\, v|_e \in \mathbb{P}_{k+2}(e),\, \partial_{\boldsymbol{n}} v|_e \in \mathbb{P}_{k+1}(e),\quad e \subset \partial K,$$
$$(v,q)_K = (\Pi_K^\nabla v, q)_K,\quad q \in \mathbb{M}_k(K)\backslash\mathbb{M}_{k-2}(K)\}.$$

### 3.2 The IP Virtual Element Spaces

The $H^1$-elliptic projection is uniquely determined by the DoFs for the $H^1$-conforming virtual element space $V_h^{1,c}$. As for the $L^2$ projection, one can use the enhancement technique to replace the additional DoFs of $v \in W_k(K)$ by the ones of $\Pi_K^\nabla v$. The local interior penalty space is then defined as

$$V_k(K) = \{v \in W_k(K) : \tilde{\chi}^g(v) = \tilde{\chi}^g(\Pi_K^\nabla v),\, \tilde{\chi}^n(v) = \tilde{\chi}^n(\Pi_K^\nabla v)\},$$

which satisfies $\Pi_K^\nabla v = v$ for $v \in \mathbb{P}_k(K)$, $\mathbb{P}_k(K) \subset V_k(K)$, and $V_k(K) \subset H^2(K)$. The associated DoFs are then given by

- $\boldsymbol{\chi}^p$ : the values of $v(z)$, $z \in \mathcal{V}_K$;
- $\boldsymbol{\chi}^e$ : the values of $v(\boldsymbol{x}_i^e)$, $i = 1, 2\ldots, k-1$, $e \subset \partial K$;
- $\boldsymbol{\chi}^K$: the moments $|K|^{-1}(m_K, v)_K$, $m_K \in \mathbb{M}_{k-2}(K)$.

Furthermore, we use $V_h$ to denote the global space of nonconforming virtual element by

$$V_h = \{v \in L^2(\Omega) : v|_K \in V_k(K),\ K \in \mathcal{T}_h,\ v\text{is continuous at each Gauss-Lobatto point}$$
$$\text{of interior edges and vanishes at each Gauss-Lobatto point of boundary edges}\}.$$

Since $V_h$ and $V_h^{1,c}$ share the same DoFs, we can introduce the interpolation from $V_h$ to $V_h^{1,c}$. For any given $v_h \in V_h$, let $I_h^c v_h$ be the nodal interpolant of $v_h$ in $V_h^{1,c}$. One can define the $H^1$-elliptic projection $\Pi_h^\nabla I_h^c v_h$ as in (3.6) and find that

$$\Pi_h^\nabla I_h^c v_h = \Pi_h^\nabla v_h,\quad v_h \in V_h, \tag{3.7}$$

since $\chi_i(I_h^c v_h) = \chi_i(v_h)$ and $\Pi_h^\nabla$ is uniquely determined by the DoFs, where $\chi_i \in \boldsymbol{\chi}$ with $\boldsymbol{\chi} = \{\boldsymbol{\chi}^p, \boldsymbol{\chi}^e, \boldsymbol{\chi}^K\}$ denoting the union of the DoFs for $V_h$.

As usual, we can define the $H^2$-projection operator $\Pi_K^{\Delta} : V_k(K) \to \mathbb{P}_k(K)$ by finding the solution $\Pi_K^{\Delta} v \in \mathbb{P}_k(K)$ of

$$\begin{cases} a^K(\Pi_K^{\Delta} v, q) = a^K(v, q), & q \in \mathbb{P}_k(K), \\ \widehat{\Pi_K^{\Delta} v} = \widehat{v}, & \widehat{\nabla \Pi_K^{\Delta} v} = \widehat{\nabla v} \end{cases}$$

for any given $v \in V_k(K)$, where the quasi-average $\widehat{v}$ is defined by

$$\widehat{v} = \frac{1}{|\partial K|} \int_{\partial K} v \mathrm{d}s.$$

Following the similar arguments in [47, Lemma 3.4] and [47, Corollary 3.6 and Corollary 3.7], we may derive the inverse inequalities, the boundedness of the $H^1$ projector and the projection error estimates described in the following Lemma.

**Lemma 3.1** *For all $v_h \in V_k(K)$ there hold*

$$|v_h|_{m,K} \lesssim h_K^{\ell-m} |v_h|_{\ell,K}, \tag{3.8}$$

$$|\Pi_K^{\nabla} v_h|_{m,K} \lesssim |v_h|_{m,K}, \tag{3.9}$$

$$|v_h - \Pi_K^{\nabla} v_h|_{\ell,K} \lesssim h_K^{\ell-m} |v_h|_{m,K}, \tag{3.10}$$

*where $m = 1, 2$ and $0 \le \ell \le m$.*

### 3.3 The IP Virtual Element Method with Modified Jump and Penalty Terms

Given the discrete bilinear form

$$a_h^K(v, w) = a^K(\Pi_K^{\Delta} v, \Pi_K^{\Delta} w) + S^K(v - \Pi_K^{\Delta} v, w - \Pi_K^{\Delta} w), \quad v, w \in V_k(K),$$

with

$$S^K(v - \Pi_K^{\Delta} v, w - \Pi_K^{\Delta} w) = h_K^{-2} \sum_{i=1}^{n_K} \chi_i(v - \Pi_K^{\Delta} v) \chi_i(w - \Pi_K^{\Delta} w),$$

where $\{\chi_i\}$ are the local DoFs on $K$ with $n_K$ being the number of the DoFs. Let

$$J_1(v, w) = \sum_{e \in \mathcal{E}_h} \frac{\lambda_e}{|e|} \int_e \Big[\frac{\partial \Pi_h^{\nabla} v}{\partial \boldsymbol{n}_e}\Big]\Big[\frac{\partial \Pi_h^{\nabla} w}{\partial \boldsymbol{n}_e}\Big] \mathrm{d}s,$$

where $\lambda_e \ge 1$ is some edge-dependent parameter, and the additional terms are given by

$$J_2(v, w) = -\sum_{e \in \mathcal{E}_h} \int_e \Big\{\frac{\partial^2 \Pi_h^{\nabla} v}{\partial \boldsymbol{n}_e^2}\Big\}\Big[\frac{\partial \Pi_h^{\nabla} w}{\partial \boldsymbol{n}_e}\Big] \mathrm{d}s,$$

$$J_3(v, w) = -\sum_{e \in \mathcal{E}_h} \int_e \Big\{\frac{\partial^2 \Pi_h^{\nabla} w}{\partial \boldsymbol{n}_e^2}\Big\}\Big[\frac{\partial \Pi_h^{\nabla} v}{\partial \boldsymbol{n}_e}\Big] \mathrm{d}s.$$

In contrast to the jump and average terms in [47], here we include the elliptic projector $\Pi_h^{\nabla}$ for all $v$ and $w$ in $J_i$ for $i = 1, 2, 3$ to simplify the implementation. According to the definition of $V_k(K)$, one easily finds that $J_2$ (or $J_3$) defined here coincides with the one given in [47], viz.,

$$J_2(v, w) = -\sum_{e \in \mathcal{E}_h} \int_e \Big\{\frac{\partial^2 \Pi_h^{\nabla} v}{\partial \boldsymbol{n}_e^2}\Big\}\Big[\frac{\partial \Pi_h^{\nabla} w}{\partial \boldsymbol{n}_e}\Big] \mathrm{d}s = -\sum_{e \in \mathcal{E}_h} \int_e \Big\{\frac{\partial^2 \Pi_h^{\nabla} v}{\partial \boldsymbol{n}_e^2}\Big\}\Big[\frac{\partial w}{\partial \boldsymbol{n}_e}\Big] \mathrm{d}s.$$

***Remark 3.1*** In Ref. [47], the penalty term is expressed as

$$J_1(v,w)=\lambda\sum_{e\in\mathcal{E}_h}\frac{1}{|e|}\int_e\Big[\frac{\partial v}{\partial \boldsymbol{n}_e}\Big]\Big[\frac{\partial w}{\partial \boldsymbol{n}_e}\Big]\mathrm{d}s, \tag{3.11}$$

where the integration can be approximated by the Gauss-Lobatto formula

$$\int_e\Big[\frac{\partial v}{\partial \boldsymbol{n}_e}\Big]\Big[\frac{\partial w}{\partial \boldsymbol{n}_e}\Big]\mathrm{d}s\approx|e|\sum_{i=0}^{k}\omega_i\Big[\frac{\partial v}{\partial \boldsymbol{n}_e}\Big](\boldsymbol{x}_i^e)\Big[\frac{\partial w}{\partial \boldsymbol{n}_e}\Big](\boldsymbol{x}_i^e)$$

with $\boldsymbol{x}_0^e$ and $\boldsymbol{x}_k^e$ being the endpoints of $e$. By the definition of $V_h$,

$$\Big[\frac{\partial v}{\partial \boldsymbol{n}_e}\Big](\boldsymbol{x}_i^e)\Big[\frac{\partial w}{\partial \boldsymbol{n}_e}\Big](\boldsymbol{x}_i^e)=\Big[\frac{\partial \Pi_h^\nabla v}{\partial \boldsymbol{n}_e}\Big](\boldsymbol{x}_i^e)\Big[\frac{\partial \Pi_h^\nabla w}{\partial \boldsymbol{n}_e}\Big](\boldsymbol{x}_i^e),\qquad i=0,k.$$

Our penalty term can be interpreted as replacing every term in the summation with the right-hand side expression for every $i$.

Our modified interior penalty virtual element methods for the problem (1.1) can be described as follows: Find $u_h\in V_h$ such that

$$\varepsilon^2\mathcal{A}_h(u_h,v_h)+b_h(u_h,v_h)=\langle f_h,v_h\rangle,\quad v_h\in V_h, \tag{3.12}$$

where

$$\mathcal{A}_h(u_h,v_h)=a_h(u_h,v_h)+J_1(u_h,v_h)+J_2(u_h,v_h)+J_3(u_h,v_h), \tag{3.13}$$

$a_h(v,w)=\sum_{K\in\mathcal{T}_h}a_h^K(v,w)$ and $b_h(v,w)=\sum_{K\in\mathcal{T}_h}b_h^K(v,w)$, with

$$b_h^K(v,w):=(\nabla\Pi_K^\nabla v,\nabla\Pi_K^\nabla w)_K+\sum_{i=1}^{n_K}\chi_i(v-\Pi_K^\nabla v)\chi_i(w-\Pi_K^\nabla w).$$

The right-hand side is

$$\langle f_h,v_h\rangle:=\sum_{K\in\mathcal{T}_h}\int_K f\,\Pi_{0,K}^k v_h\mathrm{d}x,$$

with $\Pi_{0,K}^k$ being the $L^2$ projector onto $\mathbb{P}_k(K)$.

***Remark 3.2*** In view of Eq. (3.7), we have

$$b_h^K(v,w)=b_h^K(v,I_h^c w),\quad v,w\in V_h, \tag{3.14}$$

which is crucial in the error analysis. We also have

$$b_h^K(I_h^c v,I_h^c v)=b_h^K(v,I_h^c v),\quad v,w\in V_h, \tag{3.15}$$

which implies

$$|I_h^c v_h|_{1,K}\lesssim|v_h|_{1,K}, \tag{3.16}$$

This along with (3.9), (3.10) and (3.7) gives

$$\begin{aligned}|v_h-I_h^c v_h|_{1,K}&\le|v_h-\Pi_h^\nabla v_h|_{1,K}+|\Pi_h^\nabla(v_h-I_h^c v_h)|_{1,K}\\&\lesssim|v_h-\Pi_h^\nabla v_h|_{1,K}\lesssim h_K|v_h|_{2,K}.\end{aligned} \tag{3.17}$$

By the inverse inequality for polynomials,

$$\begin{aligned} |v_h - I_h^c v_h|_{2,K} &\le |v_h - \Pi_h^\nabla v_h|_{2,K} + |\Pi_h^\nabla (v_h - I_h^c v_h)|_{2,K} \\ &\lesssim |v_h|_{2,K} + h_K^{-1} |\Pi_h^\nabla (v_h - I_h^c v_h)|_{1,K} \lesssim |v_h|_{2,K}. \end{aligned} \tag{3.18}$$

Noting that $\chi_K(I_h^c v_h) = \chi_K(v_h)$, where $\chi_K(v_h) = |K|^{-1} \int_K v_h \mathrm{d}x$, we obtain from the Poincaré-Friedrichs inequality (2.6) that

$$\|v_h - I_h^c v_h\|_{0,K} \le h_K |v_h - I_h^c v_h|_{1,K} \lesssim h_K |v_h|_{1,K}. \tag{3.19}$$

In what follows, we define

$$\|w\|_h^2 := |w|_{2,h}^2 + J_1(w, w), \qquad \|w\|_{\varepsilon,h}^2 := \varepsilon^2 \|w\|_h^2 + |w|_{1,h}^2. \tag{3.20}$$

**Lemma 3.2** *$\|\cdot\|_h$ and $\|\cdot\|_{\varepsilon,h}$ are norms on $V_h$.*

***Proof*** It is enough to prove that $\|v_h\|_h = 0$ implies $v_h = 0$ for any given $v_h \in V_h$. By definition, $\|v_h\|_h = 0$ is equivalent to

$$|v_h|_{2,h} = 0, \qquad J_1(v_h, v_h) = 0.$$

The equation $|v_h|_{2,h} = 0$ shows that $\nabla_h v_h$ is a piecewise constant on $\mathcal{T}_h$. On the other hand, the direct manipulation yields

$$\int_e \Big[\frac{\partial \Pi_h^\nabla v}{\partial \boldsymbol{n}_e}\Big]\Big[\frac{\partial \Pi_h^\nabla w}{\partial \boldsymbol{n}_e}\Big] \mathrm{d}s = \int_e \Pi_{0,e}^{k-1}\Big[\frac{\partial v}{\partial \boldsymbol{n}_e}\Big] \Pi_{0,e}^{k-1}\Big[\frac{\partial w}{\partial \boldsymbol{n}_e}\Big] \mathrm{d}s,$$

where $v, w \in V_h$. Thus, $J_1(v_h, v_h) = 0$ implies $\Pi_{0,e}^{k-1}\Big[\frac{\partial v_h}{\partial \boldsymbol{n}_e}\Big] = 0$, where $k \ge 2$. Since $\nabla_h v_h$ is piecewise constant, we further obtain $\Big[\frac{\partial v_h}{\partial \boldsymbol{n}_e}\Big] = 0$ over the edges of $\mathcal{T}_h$. That is, the normal derivative of $v_h$ is continuous over interior edges and vanishes on the boundary of $\Omega$. This reduces to the discussion in the proof of Lemma 4.2 in [47], so we omit the remaining argument. □

### 3.4 Well-Posedness of the Discrete Problem

In [47], the mesh-dependent parameter $\lambda_e$ was chosen as a sufficiently large constant $\lambda$. The stability for the bilinear forms can be obtained by using the similar arguments used in the proof of Theorem 4.3 in [47]. We omit the details with the results described as follows.

– $k$-consistency: for all $v \in V_k(K)$ and $q \in \mathbb{P}_k(K)$, it holds that

$$a_h^K(v, q) = a^K(v, q), \quad b_h^K(v, q) = b^K(v, q). \tag{3.21}$$

– Stability: there exist two positive constants $\alpha_*$ and $\alpha^*$, independent of $h$, such that

$$\alpha_* a^K(v, v) \le a_h^K(v, v) \le \alpha^* a^K(v, v), \tag{3.22}$$

$$\alpha_* b^K(v, v) \le b_h^K(v, v) \le \alpha^* b^K(v, v) \tag{3.23}$$

for all $v \in V_k(K)$.

Note that under the given mesh assumption, $\alpha_*$ and $\alpha^*$ are constants independent of the elements. Therefore, we can select the same $\alpha_*$ or $\alpha^*$ for both equations.

Here, we aim to provide an automated mesh-dependent selection of $\lambda_e$ following a similar deduction with that described in [18].

**Lemma 3.3** *For every constant $a_\lambda$ satisfying*

$$a_\lambda > \max\Big\{1, \frac{1}{\sqrt{\alpha_*}}\Big\},$$

*where $\alpha_*$ is given in (3.22), define the penalty parameter as*

$$\lambda_e = \begin{cases} \dfrac{a_\lambda C_{\nabla,e} N_K k(k-1) h_e^2}{4}\Big(\dfrac{1}{|T_+|} + \dfrac{1}{|T_-|}\Big), & e \in \mathcal{E}_h^0, \\ \dfrac{a_\lambda C_{\nabla,e} N_K k(k-1) h_e^2}{2|T_+|}, & e \in \mathcal{E}_h^\partial, \end{cases}$$

*where $C_{\nabla,e} = \max\{C_{\nabla,K_+}, C_{\nabla,K_-}\}$ with $C_{\nabla,K_\pm}$ being the hidden constants in (3.9), $T_+$ and $T_-$ are the neighboring virtual triangles for an interior edge $e \in \mathcal{E}_h^0$, $T_+$ is the adjacent virtual triangle for a boundary edge $e \in \mathcal{E}_h^\partial$, and $N_K$ is the maximum number of edges of elements. Then there holds*

$$\mathcal{A}_h(v_h, v_h) \geq \kappa \|v_h\|_h^2$$

*with the constant*

$$\kappa = \min\{\alpha_*, 1\} - \frac{1}{\sqrt{a_\lambda}}.$$

***Proof*** For every $\kappa > 0$, consider the difference

$$\begin{aligned} \mathcal{A}_h(v_h, v_h) - \kappa\|v_h\|_h^2 &= (a_h(v_h, v_h) - \kappa|v_h|_{2,h}^2) \\ &\quad + (1-\kappa)J_1(v_h, v_h) + J_2(v_h, v_h) + J_3(v_h, v_h) \\ &= (a_h(v_h, v_h) - \kappa|v_h|_{2,h}^2) + (1-\kappa)J_1(v_h, v_h) + 2J_2(v_h, v_h) \\ &\geq (\alpha_* - \kappa)|v_h|_{2,h}^2 + (1-\kappa)J_1(v_h, v_h) + 2J_2(v_h, v_h), \end{aligned}$$

where the stability (3.22) is used. For every $\epsilon > 0$, the Young's inequality gives

$$\begin{aligned} 2|J_2(v_h, v_h)| &= 2\Big|\sum_{e\in\mathcal{E}_h}\int_e \Big\{\frac{\partial^2 \Pi_h^\nabla v_h}{\partial \boldsymbol{n}_e^2}\Big\}\Big[\frac{\partial \Pi_h^\nabla v_h}{\partial \boldsymbol{n}_e}\Big]\mathrm{d}s\Big| \\ &\leq \sum_{e\in\mathcal{E}_h}\Big(\frac{\epsilon\lambda_e}{h_e}\Big\|\Big[\frac{\partial \Pi_h^\nabla v_h}{\partial \boldsymbol{n}_e}\Big]\Big\|_{0,e}^2 + \frac{h_e}{\epsilon\lambda_e}\Big\|\Big\{\frac{\partial^2 \Pi_h^\nabla v_h}{\partial \boldsymbol{n}_e^2}\Big\}\Big\|_{0,e}^2\Big) \\ &= \epsilon J_1(v_h, v_h) + \sum_{e\in\mathcal{E}_h}\frac{h_e}{\epsilon\lambda_e}\Big\|\Big\{\frac{\partial^2 \Pi_h^\nabla v_h}{\partial \boldsymbol{n}_e^2}\Big\}\Big\|_{0,e}^2. \end{aligned}$$

This reduces to the estimate of the average $\Big\{\frac{\partial^2 \Pi_h^\nabla v_h}{\partial \boldsymbol{n}_e^2}\Big\} = \Big\{\boldsymbol{n}_e^T(\nabla_h^2 \Pi_h^\nabla v_h)\boldsymbol{n}_e\Big\}$.

For an interior edge $e$ with the neighboring virtual triangles $T_+$ and $T_-$, the definition of the average and the Young's inequality give

$$\begin{aligned}\Big\|\Big\{\frac{\partial^2\Pi_h^\nabla v_h}{\partial \boldsymbol{n}_e^2}\Big\}\Big\|_{0,e}^2 &= \Big\|\frac{1}{2}\boldsymbol{n}_e^T((\nabla_h^2\Pi_h^\nabla v_h)|_{T_+}+(\nabla_h^2\Pi_h^\nabla v_h)|_{T_-})\boldsymbol{n}_e\Big\|_{0,e}^2\\ &\le \frac{1}{4}\|(\nabla_h^2\Pi_h^\nabla v_h)|_{T_+}+(\nabla_h^2\Pi_h^\nabla v_h)|_{T_-}\|_{0,e}^2\\ &= \frac{1}{4}(\|(\nabla_h^2\Pi_h^\nabla v_h)|_{T_+}\|_{0,e}^2+\|(\nabla_h^2\Pi_h^\nabla v_h)|_{T_-}\|_{0,e}^2\\ &\quad+2\int_e(\nabla_h^2\Pi_h^\nabla v_h)|_{T_+}(\nabla_h^2\Pi_h^\nabla v_h)|_{T_-}\mathrm{d}s\\ &\le \frac{1}{4}\Big((1+\alpha)\|(\nabla_h^2\Pi_h^\nabla v_h)|_{T_+}\|_{0,e}^2+(1+\frac{1}{\alpha})\|(\nabla_h^2\Pi_h^\nabla v_h)|_{T_-}\|_{0,e}^2\Big)\end{aligned} \tag{3.24}$$

for any $\alpha>0$. Since $(\nabla_h^2\Pi_h^\nabla v_h)|_{T_\pm}$ are polynomials of degree $k-2$, referring to the result in [18, 42], we derive

$$\Big\|\Big\{\frac{\partial^2\Pi_h^\nabla v_h}{\partial \boldsymbol{n}_e^2}\Big\}\Big\|_{0,e}^2\le\frac{k(k-1)h_e}{8}\Big(\frac{1+\alpha}{|T_+|}\|\nabla_h^2\Pi_h^\nabla v_h\|_{0,T_+}^2+\frac{1+1/\alpha}{|T_-|}\|\nabla_h^2\Pi_h^\nabla v_h\|_{0,T_-}^2\Big).$$

The optimal value $\alpha=|T_+|/|T_-|$ and the boundedness of $\Pi_h^\nabla$ in (3.9) of Lemma 3.1 lead to

$$\begin{aligned}\Big\|\Big\{\frac{\partial^2\Pi_h^\nabla v_h}{\partial \boldsymbol{n}_e^2}\Big\}\Big\|_{0,e}^2&\le\frac{k(k-1)h_e}{8}\Big(\frac{1}{|T_+|}+\frac{1}{|T_-|}\Big)\|\nabla_h^2\Pi_h^\nabla v_h\|_{0,T_+\cup T_-}^2\\&\le C_{\nabla,e}\frac{k(k-1)h_e}{8}\Big(\frac{1}{|T_+|}+\frac{1}{|T_-|}\Big)|v_h|_{2,K_+\cup K_-}^2.\end{aligned} \tag{3.25}$$

For a boundary edge $e$ with adjacent virtual triangle $T_+$, we can get

$$\Big\|\Big\{\frac{\partial^2\Pi_h^\nabla v_h}{\partial \boldsymbol{n}_e^2}\Big\}\Big\|_{0,e}^2\le\frac{k(k-1)h_e}{2|T_+|}\|\nabla_h^2\Pi_h^\nabla v_h\|_{0,T_+}^2\le C_{\nabla,e}\frac{k(k-1)h_e}{2|T_+|}|v_h|_{2,K_+}^2.$$

Consequently, with the choice of $\lambda_e$, the sum over all edges and the finite overlap of the edge patches lead to

$$2|J_2(v_h,v_h)|\le\epsilon J_1(v_h,v_h)+\frac{1}{a_\lambda}\epsilon|v_h|_{2,h}^2.$$

The above discussion gives

$$\mathcal{A}_h(v_h,v_h)-\kappa\|v_h\|_h^2\ge(\alpha_*-\frac{1}{a_\lambda}\epsilon-\kappa)|v_h|_{2,h}^2+(1-\epsilon-\kappa)J_1(v_h,v_h).$$

Every choice of $0<\kappa\le\min\{\alpha_*-1/(a_\lambda\epsilon),1-\epsilon\}$ leads to a nonnegative lower bound, and so proves the claim that

$$\mathcal{A}_h(v_h,v_h)\ge\kappa\|v_h\|_h^2.$$

Taking $\epsilon=1/\sqrt{a_\lambda}$ with $a_\lambda>\max\{1,\frac{1}{\sqrt{\alpha_*}}\}$ results in

$$\kappa:=\min\Big\{\alpha_*-\frac{1}{\sqrt{a_\lambda}},1-\frac{1}{\sqrt{a_\lambda}}\Big\}=\min\{\alpha_*,1\}-\frac{1}{\sqrt{a_\lambda}},$$

as required. □

***Remark 3.3*** In contrast to the finite element method discussed in [18], the parameter $\lambda_e$ for the VEM depends on the unknown constants $\alpha_*$ and $C_{\nabla,e}$. Although specifying these constants poses a challenge, they remain independent of mesh sizes under the given mesh assumption. Consequently, $\lambda_e$ can be selected proportionally to $\frac{N_K k(k-1)h_e^2}{4}\Big(\frac{1}{|T_+|}+\frac{1}{|T_-|}\Big)$ for an interior edge $e$. This also implies that the lower and upper bounds of $\lambda_e$ are also independent of mesh sizes, indicating $\lambda_e \eqsim 1$ under the given mesh assumption.

**Theorem 3.1** *For the parameter $\lambda_e$ chosen as in Lemma 3.3, there exists a unique solution to the discrete problem (3.12).*

***Proof*** For any $v_h \in V_h$, Lemma 3.3 along with the stability (3.23) yields the coercivity

$$\varepsilon^2 \mathcal{A}_h(v_h, v_h) + b_h(v_h, v_h) \geq \varepsilon^2 \kappa \|v_h\|_h^2 + \alpha_* |v_h|_{1,h}^2 \geq \min\{\kappa, \alpha_*\} \|v_h\|_{\varepsilon,h}^2 = \alpha_* \|v_h\|_{\varepsilon,h}^2, \tag{3.26}$$

For the boundedness of the bilinear form, by the definition of $\|\cdot\|_h$ given in (3.20), it suffices to consider $\varepsilon^2 J_2(v_h, w_h)$ for any $v_h, w_h \in V_h$. The Cauchy-Schwarz inequality gives

$$\begin{aligned} |J_2(v_h, w_h)| &= \Big| \sum_{e\in\mathcal{E}_h} \int_e \Big\{ \frac{\partial^2 \Pi_h^\nabla v_h}{\partial \boldsymbol{n}_e^2} \Big\} \Big[ \frac{\partial \Pi_h^\nabla w_h}{\partial \boldsymbol{n}_e} \Big] \mathrm{d}s \Big| \\ &\lesssim \Big( \sum_{e\in\mathcal{E}_h} \frac{h_e}{\lambda_e} \Big\| \Big\{ \frac{\partial^2 \Pi_h^\nabla v_h}{\partial \boldsymbol{n}_e^2} \Big\} \Big\|_e^2 \Big)^{\frac{1}{2}} \Big( \sum_{e\in\mathcal{E}_h} \frac{\lambda_e}{h_e} \Big\| \Big[ \frac{\partial \Pi_h^\nabla w_h}{\partial \boldsymbol{n}_e} \Big] \Big\|_e^2 \Big)^{\frac{1}{2}} \\ &= \Big( \sum_{e\in\mathcal{E}_h} \frac{h_e}{\lambda_e} \Big\| \Big\{ \frac{\partial^2 \Pi_h^\nabla v_h}{\partial \boldsymbol{n}_e^2} \Big\} \Big\|_e^2 \Big)^{\frac{1}{2}} J_1(w_h, w_h)^{1/2}. \end{aligned} \tag{3.27}$$

For an interior edge $e$ with the neighboring virtual triangles $T_+$ and $T_-$, we obtain from (3.25) and the definition of $\lambda_e$ that

$$\frac{h_e}{\lambda_e} \Big\| \Big\{ \frac{\partial^2 \Pi_h^\nabla v_h}{\partial \boldsymbol{n}_e^2} \Big\} \Big\|_{0,e}^2 \leq \frac{C_{\nabla,e} k(k-1) h_e^2}{8\lambda_e} \Big( \frac{1}{|T_+|} + \frac{1}{|T_-|} \Big) |v_h|_{2,K_+\cup K_-}^2 = \frac{1}{2aN_K} |v_h|_{2,K_+\cup K_-}^2,$$

where $a$ and $N_K$ are defined in Lemma 3.3. For a boundary edge $e$, one can get

$$\frac{h_e}{\lambda_e} \Big\| \Big\{ \frac{\partial^2 \Pi_h^\nabla v_h}{\partial \boldsymbol{n}_e^2} \Big\} \Big\|_{0,e}^2 \leq \frac{1}{aN_K} |v_h|_{2,K_+}^2.$$

Therefore,

$$\Big( \sum_{e\in\mathcal{E}_h} \frac{h_e}{\lambda_e} \Big\| \Big\{ \frac{\partial^2 \Pi_h^\nabla v_h}{\partial \boldsymbol{n}_e^2} \Big\} \Big\|_e^2 \Big)^{\frac{1}{2}} \lesssim |v_h|_{2,h},$$

which together with (3.27) yields

$$|\varepsilon^2 J_2(v_h, w_h)| \lesssim \|v_h\|_{\varepsilon,h} \|w_h\|_{\varepsilon,h}.$$

The proof is finished by using the Lax-Milgram lemma. □

## 4 Error Analysis

### 4.1 An Abstract Strang-Type Lemma

For any function $v \in H_0^1(\Omega) \cap H^2(\Omega)$, its interpolation $I_h v$ is defined by the condition that $v$ and $I_h v$ have the same degrees of freedom:

$$\chi_i(I_h v) = \chi_i(v), \qquad \chi_i \in \boldsymbol{\chi}.$$

Since the computation of the elliptic projection $\Pi_h^\nabla I_h u$ only involves the DoFs of $u$ and $\chi_i(I_h u) = \chi_i(u)$ for $\chi_i \in \boldsymbol{\chi}$, we define $\Pi_h^\nabla u = \Pi_h^\nabla I_h u$ in what follows, which makes the expressions $\|u - u_h\|_{\varepsilon,h}$, $\|u - I_h u\|_{\varepsilon,h}$ and $\|u - u_\pi\|_{\varepsilon,h}$ well-defined in the following lemma, where $u$ is the exact solution to (1.1).

As shown in Lemma 3.11 of [47], we can derive the following interpolation error estimate.

**Lemma 4.1** *For any $v \in H^\ell(K)$ with $2 \le \ell \le k+1$, it holds*

$$|v - I_h v|_{m,K} \lesssim h_K^{\ell-m} |v|_{\ell,K}, \quad m = 0, 1, 2, \quad K \in \mathcal{T}_h. \tag{4.1}$$

**Lemma 4.2** *Assume that $u \in H_0^2(\Omega) \cap H^s(\Omega)$ is the solution to (2.1) with $3 \le s \le k+1$. Then we have the error estimate*

$$\|u - u_h\|_{\varepsilon,h} \lesssim \|u - I_h u\|_{\varepsilon,h} + \|u - u_\pi\|_{\varepsilon,h} + \|f - f_h\|_{V_h'} + E_h(u), \tag{4.2}$$

*where $u_\pi$ is a piecewise polynomial with degree $\le k$ that satisfies (2.2),*

$$\|f - f_h\|_{V_h'} = \sup_{v_h \in V_h \setminus \{0\}} \frac{\langle f - f_h, v_h \rangle}{\|v_h\|_{\varepsilon,h}}$$

*and the consistency term*

$$E_h(u) = \sup_{v_h \in V_h \setminus \{0\}} \frac{E_A(u, v_h) + E_J(u, v_h)}{\|v_h\|_{\varepsilon,h}}, \tag{4.3}$$

*with*

$$E_A(u, v_h) = \sum_{K \in \mathcal{T}_h} (\varepsilon^2 a^K(u, v_h) + b^K(u, I_h^c v_h)) - (f, v_h),$$
$$E_J(u, v_h) = \varepsilon^2 (J_1(I_h u, v_h) + J_2(I_h u, v_h) + J_3(I_h u, v_h)),$$

*where $I_h^c$ is the conforming interpolation operator defined in Sect. 3.2.*

***Proof*** Noting that $u_\pi|_K \in V_k(K)$, we have $I_h u_\pi = u_\pi$. By the triangle inequality,

$$\|u - u_h\|_{\varepsilon,h} \le \|u - u_\pi\|_{\varepsilon,h} + \|I_h(u - u_\pi)\|_{\varepsilon,h} + \|I_h u - u_h\|_{\varepsilon,h}. \tag{4.4}$$

The interpolation error estimate in Lemma 4.1 gives

$$|I_h(u - u_\pi)|_{m,K} \le |u - u_\pi|_{m,K} + |(u - u_\pi) - I_h(u - u_\pi)|_{m,K} \lesssim |u - u_\pi|_{m,K}, \quad m = 1, 2.$$

For $\varepsilon^2 J_1(I_h(u-u_\pi), I_h(u-u_\pi))$, we obtain from Lemma 2.1 and Lemma 3.1 that

$$\begin{aligned}
&\varepsilon^2 J_1(I_h(u-u_\pi), I_h(u-u_\pi))\\
&= \varepsilon^2 \sum_{e\in\mathcal{E}_h} \frac{\lambda_e}{|e|}\int_e \Big[\frac{\partial \Pi_h^\nabla I_h(u-u_\pi)}{\partial \boldsymbol{n}_e}\Big]^2 \mathrm{d}s\\
&\lesssim \varepsilon^2 \sum_{K\in\mathcal{T}_h} \Big(|\Pi_h^\nabla(I_h u-u_\pi)|_{2,K}^2 + h_K^{-2}|\Pi_h^\nabla(I_h u-u_\pi)|_{1,K}^2\Big)\\
&\lesssim \varepsilon^2 \sum_{K\in\mathcal{T}_h} (|I_h u-u_\pi|_{2,K}^2 + h_K^{-2}|I_h u-u_\pi|_{1,K}^2) \lesssim \varepsilon^2 \sum_{K\in\mathcal{T}_h} \Big(|u-I_h u|_{2,K}^2 + |u-u_\pi|_{2,K}^2\Big),
\end{aligned}$$

where the inverse inequalities in (3.8) are used in the last step. By the definition of the norm,

$$\|I_h(u-u_\pi)\|_{\varepsilon,h} \lesssim \|u-I_h u\|_{\varepsilon,h} + \|u-u_\pi\|_{\varepsilon,h}.$$

Let $\delta_h := I_h u - u_h$. We have by the coercivity (3.26) and the definition of the discrete problem (3.12) that

$$\begin{aligned}
\alpha_*\|\delta_h\|_{\varepsilon,h}^2 &\le \varepsilon^2\Big(a_h(\delta_h,\delta_h) + J_1(\delta_h,\delta_h) + J_2(\delta_h,\delta_h) + J_3(\delta_h,\delta_h)\Big) + b_h(\delta_h,\delta_h)\\
&= \varepsilon^2\Big(a_h(I_h u,\delta_h) + J_1(I_h u,\delta_h) + J_2(I_h u,\delta_h) + J_3(I_h u,\delta_h)\Big)\\
&\quad + b_h(I_h u,\delta_h) - \langle f_h,\delta_h\rangle\\
&= \varepsilon^2 a_h(I_h u,\delta_h) + b_h(I_h u, I_h^c\delta_h) - (f,\delta_h) + \langle f-f_h,\delta_h\rangle + E_J(u,\delta_h),
\end{aligned}$$

where we have used (3.14) in Remark 3.2.

According to the $k$-consistency (3.21) and the stability formulas (3.22) and (3.23), combining with (3.16), we get

$$\begin{aligned}
&\varepsilon^2 a_h(I_h u,\delta_h) + b_h(I_h u,\delta_h) - (f,\delta_h)\\
&\quad= \sum_{K\in\mathcal{T}_h} \varepsilon^2(a_h^K(I_h u-u_\pi,\delta_h) + a^K(u_\pi-u,\delta_h))\\
&\qquad+ \sum_{K\in\mathcal{T}_h} (b_h^K(I_h u-u_\pi,\delta_h) + b^K(u_\pi-u, I_h^c\delta_h))\\
&\qquad+ \sum_{K\in\mathcal{T}_h} (\varepsilon^2 a^K(u,\delta_h) + b^K(u, I_h^c\delta_h)) - (f,\delta_h)\\
&\le \varepsilon^2(|u-I_h u|_{2,h} + |u-u_\pi|_{2,h})|\delta_h|_{2,h} + (|u-I_h u|_{1,h} + |u-u_\pi|_{1,h})|\delta_h|_{1,h} + E_A(u,\delta_h)\\
&\lesssim (\|u-I_h u\|_{\varepsilon,h} + \|u-u_\pi\|_{\varepsilon,h})\|\delta_h\|_{\varepsilon,h} + E_A(u,\delta_h).
\end{aligned}$$

The proof is completed by using the triangle inequality (4.4). □

**Lemma 4.3** *Let $u \in H_0^2(\Omega)\cap H^s(\Omega)$ with $3 \le s \le k+1$. One can get rid of $\varepsilon^2 J_2(I_h u, v_h)$ in the consistency term (4.3) and obtain*

$$\begin{aligned}
E_A(u,v_h) + E_J(u,v_h) = E_{A1}(u,v_h) + E_{A2}(u,v_h) + E_{A3}(u,v_h)\\
+ \varepsilon^2(J_1(I_h u,v_h) + J_3(I_h u,v_h)),
\end{aligned}$$

*where*

$$E_{A1}(u, v_h) = \varepsilon^2 \sum_{e\in\mathcal{E}_h} \int_e \left\{ \frac{\partial^2 (u - \Pi_h^\nabla I_h u)}{\partial \boldsymbol{n}_e^2} \right\} \left[ \frac{\partial v_h}{\partial \boldsymbol{n}_e} \right] \mathrm{d}s,$$

$$E_{A2}(u, v_h) = \varepsilon^2 \sum_{e\in\mathcal{E}_h} \int_e \frac{\partial^2 u}{\partial \boldsymbol{n}_e \partial \boldsymbol{t}_e} \left[ \frac{\partial v_h}{\partial \boldsymbol{t}_e} \right] \mathrm{d}s,$$

$$E_{A3}(u, v_h) = -\varepsilon^2 \sum_{K\in\mathcal{T}_h} (\nabla \Delta u, \nabla v_h)_K + \sum_{K\in\mathcal{T}_h} (\nabla u, \nabla I_h^c v_h)_K - (f, v_h),$$

*where $\boldsymbol{t}_e$ is a unit tangential vector of an edge $e \in \mathcal{E}_h$.*

***Proof*** For brevity, we use the summation convention whereby summation is implied when an index is repeated exactly two times. For any given $v_h \in V_h$, the integration by parts gives

$$a^K(u, v_h) = (\nabla^2 u, \nabla^2 v_h)_K = \int_K \partial_{ij} u \partial_{ij} v_h \mathrm{d}x = \int_{\partial K} \partial_{ij} u n_j \partial_i v_h \mathrm{d}s - \int_K \partial_{ijj} u \partial_i v_h \mathrm{d}x,$$

where $\boldsymbol{n}_K = (n_1, n_2)$ denotes the unit outward normal vector along the boundary $\partial K$. Since $\partial_i v = n_i \partial_{\boldsymbol{n}} v + t_i \partial_{\boldsymbol{t}} v$, we immediately obtain

$$\begin{aligned} a^K(u, v_h) &= \int_{\partial K} \partial_{ij} u n_i n_j \partial_{\boldsymbol{n}} v_h \mathrm{d}s + \int_{\partial K} \partial_{ij} u t_i n_j \partial_{\boldsymbol{t}} v_h \mathrm{d}s - \int_K \partial_{ijj} u \partial_i v_h \mathrm{d}x \\ &= \int_{\partial K} \frac{\partial^2 u}{\partial \boldsymbol{n}_K^2} \frac{\partial v_h}{\partial \boldsymbol{n}_K} \mathrm{d}s + \int_{\partial K} \frac{\partial^2 u}{\partial \boldsymbol{n}_K \partial \boldsymbol{t}_K} \frac{\partial v_h}{\partial \boldsymbol{t}_K} \mathrm{d}s - (\nabla \Delta u, \nabla v_h)_K, \end{aligned}$$

where $\boldsymbol{t}_K = (t_1, t_2)$ denotes the unit counterclockwise tangential vector along the boundary $\partial K$. Therefore,

$$\begin{aligned} E_A(u, v_h) &:= \sum_{K\in\mathcal{T}_h} (\varepsilon^2 a^K(u, v_h) + b^K(u, I_h^c v_h)) - (f, v_h) \\ &= \varepsilon^2 \sum_{e\in\mathcal{E}_h} \int_e \Big( \frac{\partial^2 u}{\partial \boldsymbol{n}_e^2} \left[ \frac{\partial v_h}{\partial \boldsymbol{n}_e} \right] + \frac{\partial^2 u}{\partial \boldsymbol{n}_e \partial \boldsymbol{t}_e} \left[ \frac{\partial v_h}{\partial \boldsymbol{t}_e} \right] \Big) \mathrm{d}s \\ &\quad - \varepsilon^2 \sum_{K\in\mathcal{T}_h} (\nabla \Delta u, \nabla v_h)_K + \sum_{K\in\mathcal{T}_h} (\nabla u, \nabla I_h^c v_h)_K - (f, v_h) \\ &=: \widetilde{E}_{A1}(u, v_h) + E_{A2}(u, v_h) + E_{A3}(u, v_h), \end{aligned} \tag{4.5}$$

where

$$\widetilde{E}_{A1}(u, v_h) = \varepsilon^2 \sum_{e\in\mathcal{E}_h} \int_e \frac{\partial^2 u}{\partial \boldsymbol{n}_e^2} \left[ \frac{\partial v_h}{\partial \boldsymbol{n}_e} \right] \mathrm{d}s,$$

and $E_{A2}(u, v_h)$ and $E_{A3}(u, v_h)$ are defined as in the lemma. For $\widetilde{E}_{A1}(u, v_h)$, we consider the decomposition

$$\begin{aligned} \widetilde{E}_{A1}(u, v_h) &= \varepsilon^2 \sum_{e\in\mathcal{E}_h} \int_e \left\{ \frac{\partial^2 (u - \Pi_h^\nabla I_h u)}{\partial \boldsymbol{n}_e^2} \right\} \left[ \frac{\partial v_h}{\partial \boldsymbol{n}_e} \right] \mathrm{d}s + \varepsilon^2 \sum_{e\in\mathcal{E}_h} \int_e \left\{ \frac{\partial^2 \Pi_h^\nabla I_h u}{\partial \boldsymbol{n}_e^2} \right\} \left[ \frac{\partial v_h}{\partial \boldsymbol{n}_e} \right] \mathrm{d}s \\ &= \varepsilon^2 \sum_{e\in\mathcal{E}_h} \int_e \left\{ \frac{\partial^2 (u - \Pi_h^\nabla I_h u)}{\partial \boldsymbol{n}_e^2} \right\} \left[ \frac{\partial v_h}{\partial \boldsymbol{n}_e} \right] \mathrm{d}s - \varepsilon^2 J_2(I_h u, v_h) \\ &= E_{A1}(u, v_h) - \varepsilon^2 J_2(I_h u, v_h). \end{aligned}$$

The result follows from Lemma 4.2. □

### 4.2 Error Estimate

For $3 \le s \le k+1$, the estimate of the load term is

$$\begin{aligned}\langle f - f_h, v_h\rangle &= \sum_{K\in\mathcal{T}_h} (f, v_h - \Pi^k_{0,K} v_h)_K = \sum_{K\in\mathcal{T}_h} (f - \Pi^{s-3}_{0,K} f, v_h - \Pi^k_{0,K} v_h)_K \\ &\lesssim \sum_{K\in\mathcal{T}_h} h_K^{s-2} |f|_{s-2,K} h_K |v_h|_{1,K} \lesssim h^{s-1} |f|_{s-2} \|v_h\|_{\varepsilon,h}, \end{aligned} \tag{4.6}$$

namely,

$$\|f - f_h\|_{V_h'} \lesssim h^{s-1} |f|_{s-2}. \tag{4.7}$$

Replacing $\Pi^{s-3}_{0,K} f$ by 0, one also easily finds that

$$\|f - f_h\|_{V_h'} \lesssim h \|f\|. \tag{4.8}$$

We now consider the consistency term in Lemma 4.2.

**Lemma 4.4** *Given $k \ge 2$ and $f \in H^{s-2}(\Omega)$ with $3 \le s \le k+1$, assume that $u \in H^2_0(\Omega) \cap H^s(\Omega)$ is the solution of (2.1) for $s = 3$, and it is the solution of (1.1) for $s \ge 4$, respectively. Then the consistency error is bounded by*

$$E_h(u) \lesssim \begin{cases} (h^{s-1} + \varepsilon h^{s-2})|u|_s + h^{s-1}|f|_{s-2}, \\ h^{s-2}(|u|_{s-1} + \varepsilon |u|_s) + h^{s-1}|f|_{s-2}. \end{cases} \tag{4.9}$$

***Proof*** For clarity, we divide the proof into two steps.

Step 1: According to Lemma 4.3, one has

$$\begin{aligned} E_A(u, v_h) + E_J(u, v_h) &= E_{A1}(u, v_h) + E_{A2}(u, v_h) + E_{A3}(u, v_h) \\ &\quad + \varepsilon^2 (J_1(I_h u, v_h) + J_3(I_h u, v_h)), \end{aligned} \tag{4.10}$$

where $E_{A1}(u, v_h)$ can be decomposed as the sum of $E^1_{A1}(u, v_h)$ and $E^2_{A1}(u, v_h)$, with

$$\begin{aligned} E^1_{A1}(u, v_h) &= \varepsilon^2 \sum_{e\in\mathcal{E}_h} \int_e \left\{ \frac{\partial^2 (u - \Pi^\nabla_h I_h u)}{\partial \boldsymbol{n}_e^2} \right\} \left[ \frac{\partial (v_h - \Pi^\nabla_h v_h)}{\partial \boldsymbol{n}_e} \right] \mathrm{d}s, \\ E^2_{A1}(u, v_h) &= \varepsilon^2 \sum_{e\in\mathcal{E}_h} \int_e \left\{ \frac{\partial^2 (u - \Pi^\nabla_h I_h u)}{\partial \boldsymbol{n}_e^2} \right\} \left[ \frac{\partial \Pi^\nabla_h v_h}{\partial \boldsymbol{n}_e} \right] \mathrm{d}s. \end{aligned}$$

Applying the Cauchy-Schwarz inequality, the trace inequality and the projection error estimates, we can get

$$\begin{aligned}
E_{A1}^1(u, v_h) &= \varepsilon^2 \sum_{e\in\mathcal{E}_h} \int_e \Big\{ \frac{\partial^2(u-\Pi_h^\nabla I_h u)}{\partial \boldsymbol{n}_e^2} \Big\} \Big[ \frac{\partial(v_h-\Pi_h^\nabla v_h)}{\partial \boldsymbol{n}_e} \Big] \mathrm{d}s \\
&\le \varepsilon^2 \sum_{e\in\mathcal{E}_h} \Big\| \Big\{ \frac{\partial^2(u-\Pi_h^\nabla I_h u)}{\partial \boldsymbol{n}_e^2} \Big\} \Big\|_{0,e} \Big\| \Big[ \frac{\partial(v_h-\Pi_h^\nabla v_h)}{\partial \boldsymbol{n}_e} \Big] \Big\|_{0,e} \\
&\lesssim \varepsilon^2 \sum_{K\in\mathcal{T}_h} \Big( h_K^{1/2} |u-\Pi_h^\nabla I_h u|_{3,K} + h_K^{-1/2} |u-\Pi_h^\nabla I_h u|_{2,K} \Big) \\
&\quad \times \Big( h_K^{1/2} |v_h-\Pi_h^\nabla v_h|_{2,K} + h_K^{-1/2} |v_h-\Pi_h^\nabla v_h|_{1,K} \Big) \\
&\lesssim \varepsilon^2 \sum_{K\in\mathcal{T}_h} \Big( h_K |u-\Pi_h^\nabla I_h u|_{3,K} + |u-\Pi_h^\nabla I_h u|_{2,K} \Big) |v_h|_{2,K}.
\end{aligned}$$

The inverse inequality for polynomials and the boundedness of $\Pi_h^\nabla$ in (3.9) imply

$$\begin{aligned}
&h_K |u-\Pi_h^\nabla I_h u|_{3,K} + |u-\Pi_h^\nabla I_h u|_{2,K} \\
&\le h_K |u-u_\pi|_{3,K} + h_K |\Pi_h^\nabla (I_h u - u_\pi)|_{3,K} + |u-u_\pi|_{2,K} + |\Pi_h^\nabla (I_h u - u_\pi)|_{2,K} \\
&\lesssim h_K |u-u_\pi|_{3,K} + |I_h u - u_\pi|_{2,K} + |u-u_\pi|_{2,K} + |I_h u - u_\pi|_{2,K} \\
&\lesssim |u-I_h u|_{2,K} + |u-u_\pi|_{2,K} + h_K |u-u_\pi|_{3,K}.
\end{aligned}$$

This together with the Dupont-Scott theory, the Cauchy-Schwarz inequality and Lemma 4.1 gives

$$\begin{aligned}
E_{A1}^1(u, v_h) &\lesssim \varepsilon (|u-I_h u|_{2,h} + |u-u_\pi|_{2,h} + h|u-u_\pi|_{3,h}) \|v_h\|_{\varepsilon,h} \\
&\lesssim \varepsilon h^{s-2} |u|_s \|v_h\|_{\varepsilon,h}.
\end{aligned}$$

According to the Cauchy-Schwarz inequality,

$$\begin{aligned}
E_{A1}^2(u, v_h) &= \varepsilon^2 \sum_{e\in\mathcal{E}_h} \int_e \Big\{ \frac{\partial^2(u-\Pi_h^\nabla I_h u)}{\partial \boldsymbol{n}_e^2} \Big\} \Big[ \frac{\partial \Pi_h^\nabla v_h}{\partial \boldsymbol{n}_e} \Big] \mathrm{d}s \\
&\le \varepsilon^2 \Big( \sum_{e\in\mathcal{E}_h} \frac{h_e}{\lambda_e} \Big\| \Big\{ \frac{\partial^2(u-\Pi_h^\nabla I_h u)}{\partial \boldsymbol{n}_e^2} \Big\} \Big\|_e^2 \Big)^{1/2} J_1(v_h, v_h)^{1/2}.
\end{aligned}$$

The trace inequality, the inverse inequality on polynomials, the boundedness of $\Pi_h^\nabla$ in (3.9), and $\lambda_e \eqsim 1$ give

$$\begin{aligned}
&\Big( \sum_{e\in\mathcal{E}_h} \frac{h_e}{\lambda_e} \Big\| \Big\{ \frac{\partial^2(u-\Pi_h^\nabla I_h u)}{\partial \boldsymbol{n}_e^2} \Big\} \Big\|_e^2 \Big)^{1/2} \\
&\lesssim \Big[ \sum_{e\in\mathcal{E}_h} h_e \Big( \Big\| \Big\{ \frac{\partial^2(u-u_\pi)}{\partial \boldsymbol{n}_e^2} \Big\} \Big\|_e^2 + \Big\| \Big\{ \frac{\partial^2(u_\pi-\Pi_h^\nabla I_h u)}{\partial \boldsymbol{n}_e^2} \Big\} \Big\|_e^2 \Big) \Big]^{1/2} \\
&\lesssim \Big[ \sum_{K\in\mathcal{T}_h} (|u-u_\pi|_{2,K}^2 + h_K^2 |u-u_\pi|_{3,K}^2 + |\Pi_h^\nabla (I_h u - u_\pi)|_{2,K}^2) \Big]^{1/2} \\
&\lesssim |u-I_h u|_{2,h} + |u-u_\pi|_{2,h} + h|u-u_\pi|_{3,h}.
\end{aligned}$$

This along with the Dupont-Scott theory and Lemma 4.1 yields

$$\begin{aligned} E_{A1}^2(u, v_h) &\lesssim \varepsilon^2(|u - I_h u|_{2,h} + |u - u_\pi|_{2,h} + h|u - u_\pi|_{3,h}) J_1(v_h, v_h)^{1/2} \\ &\lesssim \varepsilon h^{s-2}|u|_s \|v_h\|_{\varepsilon,h}. \end{aligned}$$

Collecting above estimates to derive

$$E_{A1}(u, v_h) = E_{A1}^1(u, v_h) + E_{A1}^2(u, v_h) \lesssim \varepsilon h^{s-2}|u|_s \|v_h\|_{\varepsilon,h}.$$

For $E_{A2}(u, v_h)$, similar to the arguments in [48, Lemma 5.3], one has

$$E_{A2}(u, v_h) \lesssim \varepsilon^2 h^{s-2}|u|_s |v_h|_{2,h} \lesssim \varepsilon h^{s-2}|u|_s \|v_h\|_{\varepsilon,h}.$$

We next estimate

$$E_{A3}(u, v_h) = -\varepsilon^2 \sum_{K\in\mathcal{T}_h} (\nabla\Delta u, \nabla v_h)_K + \sum_{K\in\mathcal{T}_h} (\nabla u, \nabla I_h^c v_h)_K - (f, v_h). \tag{4.11}$$

When $s = 3$ or $k = 2$, the solution $u \in H_0^2(\Omega) \cap H^3(\Omega)$ is assumed to be the solution to (2.1). By definition,

$$\varepsilon^2 a(u, \varphi) + b(u, \varphi) = (f, \varphi), \quad \varphi \in C_0^\infty(\Omega).$$

The integration by parts gives

$$-\varepsilon^2(\nabla(\Delta u), \nabla\varphi) + (\nabla u, \nabla\varphi) = (f, \varphi), \quad \varphi \in C_0^\infty(\Omega),$$

which implies

$$-\varepsilon^2 \sum_{K\in\mathcal{T}_h} (\nabla(\Delta u), \nabla I_h^c v_h)_K + \sum_{K\in\mathcal{T}_h} (\nabla u, \nabla I_h^c v_h)_K = (f, I_h^c v_h)$$

since $C_0^\infty(\Omega)$ is dense in $H_0^1(\Omega)$, $u \in H^3(\Omega)$ and $I_h^c v_h \in H_0^1(\Omega)$. Hence,

$$E_{A3}(u, v_h) = \sum_{K\in\mathcal{T}_h} \varepsilon^2\big(\nabla\Delta u, \nabla(I_h^c v_h - v_h)\big)_K + (f, I_h^c v_h - v_h). \tag{4.12}$$

Noting that $\chi_K(I_h^c v_h) = \chi_K(v_h)$, where $\chi_K(v) = \int_K v\mathrm{d}x/|K|$, one has $\Pi_{0,K}^0 I_h^c v_h = \Pi_{0,K}^0 v_h$, yielding

$$(f, I_h^c v_h - v_h)_K = (f - \Pi_{0,K}^0 f, I_h^c v_h - v_h)_K.$$

By the Dupont-Scott theory and the estimates in (3.17) and (3.19),

$$\begin{aligned} E_{A3}(u, v_h) &\lesssim \sum_{K\in\mathcal{T}_h} (\varepsilon^2|u|_{3,K}|I_h^c v_h - v_h|_{1,K} + h_K|f|_{1,K}\|I_h^c v_h - v_h\|_{0,K}) \\ &\lesssim \sum_{K\in\mathcal{T}_h} (\varepsilon^2 h_K|u|_{3,K}|v_h|_{2,K} + h_K^2|f|_{1,K}|v_h|_{1,K}) \\ &\lesssim (\varepsilon h|u|_3 + h|f|_1)\|v_h\|_{\varepsilon,h} = h^{s-2}(\varepsilon|u|_3 + h|f|_{s-2})\|v_h\|_{\varepsilon,h}, \qquad s = 3. \end{aligned}$$

When $s \geq 4$ or $k \geq 3$, the solution $u \in H_0^2(\Omega) \cap H^s(\Omega)$ is assumed to be the solution to (1.1). In this case, one can simply use the first equation in (1.1) to get

$$\begin{aligned} 0 &= \varepsilon^2(\Delta^2 u, I_h^c v_h) - (\Delta u, I_h^c v_h) - (f, I_h^c v_h) \\ &= -\varepsilon^2 \sum_{K\in\mathcal{T}_h} (\nabla(\Delta u), \nabla I_h^c v_h)_K + \sum_{K\in\mathcal{T}_h} (\nabla u, \nabla I_h^c v_h)_K - (f, I_h^c v_h), \end{aligned}$$

where the jump terms arising from the integration by parts vanish since $I_h^c v_h$ is continuous, which also implies (4.12). Recalling the continuity of $v_h$ at the vertices and Gauss-Lobatto points, we conclude that the quadrature formula is exact for polynomials of up to degree $(2k-1)$, which means

$$\int_e q[v_h]\mathrm{d}s = 0, \quad q \in \mathbb{P}_{k-3}(e), \ e \in \mathcal{E}_h. \tag{4.13}$$

By the integration by parts in (4.12), along with the original equation (1.1) and $[I_h^c v_h]|_e = 0$, it yields

$$E_{A3}(u, v_h) = -\sum_{K\in\mathcal{T}_h} (\Delta u, I_h^c v_h - v_h)_K - \varepsilon^2 \sum_{e\in\mathcal{E}_h} \int_e \frac{\partial \Delta u}{\partial \boldsymbol{n}_e}[v_h]\mathrm{d}s.$$

Noting that

$$\chi_K(I_h^c v_h) = \chi_K(v_h) \quad \text{or} \quad (m_K, I_h^c v_h)_K = (m_K, v_h)_K \quad \text{for every} \quad m_K \in \mathbb{M}_{k-2}(K),$$

we have $(\Pi_{0,K}^{\ell}\Delta u, I_h^c v_h - v_h)_K = 0$ with $0 \le \ell \le k-2$, which yields

$$\begin{aligned} E_{A3}(u, v_h) &= -\sum_{K\in\mathcal{T}_h} (\Delta u, I_h^c v_h - v_h)_K - \sum_{e\in\mathcal{E}_h} \varepsilon^2 \int_e \frac{\partial \Delta u}{\partial \boldsymbol{n}_e}[v_h]\mathrm{d}s \\ &= -\sum_{K\in\mathcal{T}_h} (\Delta u - \Pi_{0,K}^{\ell}\Delta u, I_h^c v_h - v_h)_K \\ &\quad - \sum_{e\in\mathcal{E}_h} \varepsilon^2 \int_e \Big(\frac{\partial \Delta u}{\partial \boldsymbol{n}_e} - q_e\Big)[v_h - I_h^c v_h]\mathrm{d}s, \quad q_e \in \mathbb{P}_{k-3}(e). \end{aligned}$$

The standard argument from [25, 48] leads to

$$\Big\| \frac{\partial \Delta u}{\partial \boldsymbol{n}_e} - \Pi_{0,e}^{s-4}\frac{\partial \Delta u}{\partial \boldsymbol{n}_e} \Big\|_e \lesssim h_K^{s-7/2}|u|_{s,K}, \quad s \ge 4, \ e \subset \partial K,$$

with $\Pi_{0,e}^{s-4}$ being the $L^2$ projector onto $\mathbb{P}_{s-4}(e)$. With $q_e = \Pi_{0,e}^{s-4}\frac{\partial \Delta u}{\partial \boldsymbol{n}_e} \in \mathbb{P}_{k-3}(e)$, combining the trace inequality, Lemma 4.1, (4.13), and the Cauchy-Schwarz inequality, we derive

$$\begin{aligned} \Big| -\sum_{e\in\mathcal{E}_h} \varepsilon^2 \int_e \Big(\frac{\partial \Delta u}{\partial \boldsymbol{n}_e} - q_e\Big)[v_h - I_h^c v_h]\mathrm{d}s \Big| &\lesssim \sum_{K\in\mathcal{T}_h} \varepsilon^2 h_K^{s-7/2}|u|_{s,K} h_K^{3/2}|v_h|_{2,K} \\ &\lesssim \varepsilon h^{s-2}|u|_s \|v_h\|_{\varepsilon,h}. \end{aligned}$$

Apply the Cauchy-Schwarz inequality, the Dupont-Scott theory and (3.19) to get

$$\begin{aligned} \Big| -\sum_{K\in\mathcal{T}_h} (\Delta u - \Pi_{0,K}^{\ell}\Delta u, I_h^c v_h - v_h)_K \Big| &\lesssim \sum_{K\in\mathcal{T}_h} h_K^{\ell+1}|\Delta u|_{\ell+1} h_K |v_h|_{1,K} \\ &\lesssim h^{\ell+2}|u|_{\ell+3}\|v_h\|_{\varepsilon,h}, \end{aligned}$$

where $\ell$ can be chosen as $s-3$ or $s-4$ since it gives $0 \le \ell \le k-2$ when $4 \le s \le k+1$. Combining the above two inequalities yields

$$E_{A3}(u, v_h) \lesssim \begin{cases} (h^{s-1} + \varepsilon h^{s-2})|u|_s + h^{s-1}|f|_{s-2}, & \ell = s-3, \\ h^{s-2}(|u|_{s-1} + \varepsilon|u|_s) + h^{s-1}|f|_{s-2}, & \ell = s-4. \end{cases}$$

Step 2: The remaining is to discuss $\varepsilon^2 J_1(I_h u, v_h)$ and $\varepsilon^2 J_3(I_h u, v_h)$. For $\varepsilon^2 J_1(I_h u, v_h)$, the continuity of $u$ leads to

$$\begin{aligned}\varepsilon^2 J_1(I_h u, v_h) &= \varepsilon^2 \sum_{e\in\mathcal{E}_h} \frac{\lambda_e}{|e|} \int_e \Big[\frac{\partial \Pi_h^\nabla I_h u}{\partial \boldsymbol{n}_e}\Big]\Big[\frac{\partial \Pi_h^\nabla v_h}{\partial \boldsymbol{n}_e}\Big] \mathrm{d}s \\ &= \varepsilon^2 \sum_{e\in\mathcal{E}_h} \frac{\lambda_e}{|e|} \int_e \Big[\frac{\partial (\Pi_h^\nabla I_h u - u)}{\partial \boldsymbol{n}_e}\Big]\Big[\frac{\partial \Pi_h^\nabla v_h}{\partial \boldsymbol{n}_e}\Big] \mathrm{d}s \\ &\le \varepsilon^2 \Big( \sum_{e\in\mathcal{E}_h} \frac{\lambda_e}{|e|} \Big\| \Big[\frac{\partial (\Pi_h^\nabla I_h u - u)}{\partial \boldsymbol{n}_e}\Big] \Big\|_{0,e}^2 \Big)^{1/2} J_1(v_h, v_h)^{1/2}.\end{aligned}$$

As for the estimate of $E_{A1}^1(u, v_h)$, this further gives

$$\begin{aligned}\varepsilon^2 J_1(I_h u, v_h) &\lesssim \varepsilon \Big( \sum_{K\in\mathcal{T}_h} |\Pi_h^\nabla I_h u - u|_{2,K}^2 + h_K^{-2} |\Pi_h^\nabla I_h u - u|_{1,K}^2 \Big)^{1/2} \|v_h\|_{\varepsilon,h} \\ &\lesssim \varepsilon \Big( \sum_{K\in\mathcal{T}_h} |u - I_h u|_{2,K}^2 + |u - u_\pi|_{2,K}^2 + h_K^{-2} (|u - I_h u|_{1,K}^2 + |u - u_\pi|_{1,K}^2) \Big)^{1/2} \|v_h\|_{\varepsilon,h} \\ &\lesssim \varepsilon h^{s-2} |u|_s \|v_h\|_{\varepsilon,h}.\end{aligned}$$

For $\varepsilon^2 J_3(I_h u, v_h)$, the continuity of $u$, the trace inequality, the inverse inequality for polynomials, the boundedness of $\Pi_h^\nabla$ in (3.9) and the Cauchy-Schwarz inequality give

$$\begin{aligned}&\varepsilon^2 J_3(I_h u, v_h) \\ &= \varepsilon^2 \sum_{e\in\mathcal{T}_h} \int_e \Big[\frac{\partial (\Pi_h^\nabla I_h u - u)}{\partial \boldsymbol{n}_e}\Big]\Big[\frac{\partial^2 \Pi_h^\nabla v_h}{\partial \boldsymbol{n}_e^2}\Big] \mathrm{d}s \lesssim \varepsilon^2 \sum_{e\in\mathcal{T}_h} \Big\| \Big[\frac{\partial (\Pi_h^\nabla I_h u - u)}{\partial \boldsymbol{n}_e}\Big] \Big\|_{0,e} \Big\| \Big[\frac{\partial^2 \Pi_h^\nabla v_h}{\partial \boldsymbol{n}_e^2}\Big] \Big\|_{0,e} \\ &\lesssim \varepsilon^2 \sum_{K\in\mathcal{T}_h} \Big( h_K^{1/2} |\Pi_h^\nabla I_h u - u|_{2,K} + h_K^{-1/2} |\Pi_h^\nabla I_h u - u|_{1,K} \Big) \Big( h_K^{-1/2} |\Pi_h^\nabla v_h|_{2,K} + h_K^{1/2} |\Pi_h^\nabla v_h|_{3,K} \Big) \\ &\lesssim \varepsilon^2 \sum_{K\in\mathcal{T}_h} \Big( |\Pi_h^\nabla I_h u - u|_{2,K} + h_K^{-1} |\Pi_h^\nabla I_h u - u|_{1,K} \Big) \Big( |\Pi_h^\nabla v_h|_{2,K} + h_K |\Pi_h^\nabla v_h|_{3,K} \Big) \\ &\lesssim \varepsilon^2 \sum_{K\in\mathcal{T}_h} \Big( |u - I_h u|_{2,K} + |u - u_\pi|_{2,k} + h_K^{-1} (|u - I_h u|_{1,k} + |u - u_\pi|_{1,K}) \Big) |v_h|_{2,K} \\ &\lesssim \varepsilon^2 \sum_{K\in\mathcal{T}_h} h_K^{s-2} |u|_{s,K} |v_h|_{2,K} \lesssim \varepsilon h^{s-2} |u|_s \|v_h\|_{\varepsilon,h}.\end{aligned}$$

The proof is completed by combining the estimates in the above two steps. □

To sum up the above results, we obtain the error estimate for the mIPVEM described as follows.

**Theorem 4.1** *Under the assumption of Lemma 4.4, there holds*

$$\|u - u_h\|_{\varepsilon,h} \lesssim \begin{cases} (h^{s-1} + \varepsilon h^{s-2}) |u|_s + h^{s-1} |f|_{s-2}, \\ h^{s-2} (|u|_{s-1} + \varepsilon |u|_s) + h^{s-1} |f|_{s-2}. \end{cases}$$

***Proof*** We only need to bound each term of the right-hand side of (4.2) in Lemma 4.2. By the trace inequality, the boundedness of $\Pi_h^\nabla$ in (3.9), the interpolation error estimate in Lemma 4.1 and the Dupont-Scott theory, there exists $u_\pi \in \mathbb{P}_k(\mathcal{T}_h)$ such that

$$\|u - I_h u\|_{\varepsilon,h} + \|u - u_\pi\|_{\varepsilon,h} \lesssim h^{\ell-1} |u|_\ell + \varepsilon h^{\ell'-2} |u|_{\ell'}, \qquad 2 \le \ell, \ell' \le k+1.$$

If $\ell = \ell' = s$, then

$$\|u - I_h u\|_{\varepsilon,h} + \|u - u_\pi\|_{\varepsilon,h} \lesssim (h^{s-1} + \varepsilon h^{s-2})|u|_s.$$

If $\ell = s - 1$, $\ell' = s$, then

$$\|u - I_h u\|_{\varepsilon,h} + \|u - u_\pi\|_{\varepsilon,h} \lesssim h^{s-2}(|u|_{s-1} + \varepsilon|u|_s).$$

The proof is completed by combining the above equations, (4.7) and Lemma 4.4. □

### 4.3 Uniform Error Estimate in the Lowest Order Case

Let $u^0$ be the solution of the following boundary value problem:

$$\begin{cases} -\Delta u^0 = f & \text{in } \Omega \\ u^0 = 0 & \text{on } \partial\Omega. \end{cases} \tag{4.14}$$

The following regularity is well-known and can be found in [33] for instance.

**Lemma 4.5** *If $\Omega$ is a bounded convex polygonal domain, then*

$$|u|_2 + \varepsilon|u|_3 \lesssim \varepsilon^{-1/2}\|f\| \quad \text{and} \quad |u - u^0|_1 \lesssim \varepsilon^{1/2}\|f\|$$

*for all $f \in L^2(\Omega)$.*

**Theorem 4.2** *Let $k = 2$ be the order of the virtual element space. Assume that $f \in L^2(\Omega)$ and $u \in H_0^2(\Omega) \cap H^3(\Omega)$ is the solution to (2.1). If $\Omega$ is a bounded convex polygonal domain, then*

$$\|u - u_h\|_{\varepsilon,h} \lesssim h^{1/2}\|f\|. \tag{4.15}$$

***Proof*** We only need to estimate the right-hand side of (4.2) in Lemma 4.2 term by term.

Step 1:Similar to the procedure in [45, Theorem 4.3], we have

$$|u - I_h u|_{1,h} \lesssim h^{1/2}\|f\|, \quad \varepsilon|u - I_h u|_{2,h} \lesssim h^{1/2}\|f\|, \tag{4.16}$$

$$|u - u_\pi|_{1,h} \lesssim h^{1/2}\|f\|, \quad \varepsilon|u - u_\pi|_{2,h} \lesssim h^{1/2}\|f\|, \tag{4.17}$$

where the derivation involves the boundary value problem (4.14) and the second estimate in Lemma 4.5. Notice that $\Pi_h^\nabla u = \Pi_h^\nabla I_h u$, which means

$$J_1(u - I_h u, u - I_h u) = 0. \tag{4.18}$$

On the other hand, by the trace inequality (2.3) and the boundedness of $\Pi_h^\nabla$, $\lambda_e \eqsim 1$, combining with (2.2) and Lemma 4.5, one gets

$$\begin{aligned} &\varepsilon^2 J_1(u - u_\pi, u - u_\pi) \\ &\quad \le \varepsilon^2 \sum_{e\in\mathcal{E}_h} \frac{\lambda_e}{|e|} \left\| \left[ \frac{\partial \Pi_h^\nabla (u - u_\pi)}{\partial \boldsymbol{n}_e} \right] \right\|_e^2 \\ &\quad \lesssim \varepsilon^2 \sum_{K\in\mathcal{T}_h} \frac{\lambda_e}{|e|} \left( |\Pi_h^\nabla (u - u_\pi)|_{1,K}^2 + |\Pi_h^\nabla (u - u_\pi)|_{1,K} |\Pi_h^\nabla (u - u_\pi)|_{2,K} \right) \\ &\quad \lesssim \varepsilon^2 \sum_{K\in\mathcal{T}_h} \frac{\lambda_e}{|e|} (h_K^2 |u|_{2,K}^2 + h_K^2 |u|_{2,K} |u|_{3,K}) \lesssim \varepsilon^2 h(|u|_2^2 + |u|_2|u|_3) \lesssim h\|f\|^2. \end{aligned} \tag{4.19}$$

By the definition of the norm, we obtain from (4.16)–(4.19) that

$$\|u - I_h u\|_{\varepsilon,h} + \|u - u_\pi\|_{\varepsilon,h} \lesssim h^{1/2}\|f\|. \tag{4.20}$$

The estimate of $\|f - f_h\|_{V_h'}$ on the right-hand side of (4.2) is given in (4.8).

Step 2: For the consistency term, we first consider $E_{A1}(u, v_h)$, $E_{A2}(u, v_h)$, $E_{A3}(u, v_h)$ defined in Lemma 4.3. By the trace inequalities in Lemma 2.1,

$$\begin{aligned}
E^1_{A1}(u, v_h) &= \varepsilon^2 \sum_{e\in\mathcal{E}_h} \int_e \Big\{ \frac{\partial^2(u - \Pi_h^\nabla I_h u)}{\partial \boldsymbol{n}_e^2} \Big\} \Big[ \frac{\partial(v_h - \Pi_h^\nabla v_h)}{\partial \boldsymbol{n}_e} \Big] \mathrm{d}s \\
&\lesssim \varepsilon^2 \sum_{e\in\mathcal{E}_h} \Big\| \Big\{ \frac{\partial^2(u - \Pi_h^\nabla I_h u)}{\partial \boldsymbol{n}_e^2} \Big\} \Big\|_e \Big\| \Big[ \frac{\partial(v_h - \Pi_h^\nabla v_h)}{\partial \boldsymbol{n}_e} \Big] \Big\|_e \\
&\lesssim \varepsilon^2 \sum_{K\in\mathcal{T}_h} \Big( |u - \Pi_h^\nabla I_h u|_{2,K} + |u - \Pi_h^\nabla I_h u|_{2,K}^{1/2} |u - \Pi_h^\nabla I_h u|_{3,K}^{1/2} \Big) \\
&\quad \times \Big( h_K^{1/2} |v_h - \Pi_h^\nabla v_h|_{2,K} + h_K^{-1/2} |v_h - \Pi_h^\nabla v_h|_{1,K} \Big).
\end{aligned} \tag{4.21}$$

This along with the boundedness of $\Pi_h^\nabla$, the interpolation error estimate in Lemma 4.1, the projection error estimates in Lemma 3.1 and Lemma 4.5 gives

$$\begin{aligned}
E^1_{A1}(u, v_h) &\lesssim \varepsilon^2 \sum_{K\in\mathcal{T}_h} \Big( |u|_{2,K} + |u|_{2,K}^{1/2} |u|_{3,K}^{1/2} \Big) h_K^{1/2} |v_h|_{2,K} \\
&\lesssim \varepsilon h^{1/2} \Big[ \Big( \sum_{K\in\mathcal{T}_h} |u|_{2,K}^2 \Big)^{1/2} + \Big( \sum_{K\in\mathcal{T}_h} |u|_{2,K} |u|_{3,K} \Big)^{1/2} \Big] \|v_h\|_{\varepsilon,h} \\
&\lesssim \varepsilon h^{1/2} \Big( |u|_2 + |u|_2^{1/2} |u|_3^{1/2} \Big) \|v_h\|_{\varepsilon,h} \lesssim h^{1/2} \|f\| \|v_h\|_{\varepsilon,h}.
\end{aligned} \tag{4.22}$$

Similar to the derivation of (4.22), we can obtain

$$E^2_{A1}(u, v_h) = \varepsilon^2 \sum_{e\in\mathcal{E}_h} \int_e \Big\{ \frac{\partial^2(u - \Pi_h^\nabla I_h u)}{\partial \boldsymbol{n}_e^2} \Big\} \Big[ \frac{\partial \Pi_h^\nabla v_h}{\partial \boldsymbol{n}_e} \Big] \mathrm{d}s \lesssim h^{1/2} \|f\| \|v_h\|_{\varepsilon,h}.$$

Therefore,

$$E_{A1}(u, v_h) = E^1_{A1}(u, v_h) + E^2_{A1}(u, v_h) \lesssim h^{1/2} \|f\| \|v_h\|_{\varepsilon,h}.$$

For $E_{A2}(u, v_h)$, we first obtain from the continuity of $v_h$ at vertices that

$$\int_e q \Big[ \frac{\partial v_h}{\partial \boldsymbol{t}_e} \Big] \mathrm{d}s = - \int_e \frac{\partial q}{\partial \boldsymbol{t}_e} [v_h] \mathrm{d}s = 0, \quad q \in \mathbb{P}_0(e), \quad e \in \mathcal{E}_h.$$

By setting $w|_e = \dfrac{\partial^2 u}{\partial \boldsymbol{n}_e \partial \boldsymbol{t}_e} = \boldsymbol{n_e}^T \nabla^2 u \boldsymbol{t}_e$, where $w$ is extended outside $e$ so that $\boldsymbol{n}_e$ and $\boldsymbol{t}_e$ are constant along the lines perpendicular to $e$, this implies

$$\begin{aligned}
E_{A2}(u, v_h) &= \varepsilon^2 \sum_{e\in\mathcal{E}_h} \int_e \Big( \frac{\partial^2 u}{\partial \boldsymbol{n}_e \partial \boldsymbol{t}_e} - \Pi^0_{0,e} \Big( \frac{\partial^2 u}{\partial \boldsymbol{n}_e \partial \boldsymbol{t}_e} \Big) \Big) \Big( \Big[ \frac{\partial v_h}{\partial \boldsymbol{t}_e} \Big] - \Pi^0_{0,e} \Big[ \frac{\partial v_h}{\partial \boldsymbol{t}_e} \Big] \Big) \mathrm{d}s \\
&\le \varepsilon^2 \sum_{e\in\mathcal{E}_h} \|w - \Pi^0_{0,e} w\|_e \|[\partial_{\boldsymbol{t}_e} v_h] - \Pi^0_{0,e} [\partial_{\boldsymbol{t}_e} v_h]\|_e \\
&\le \varepsilon^2 \sum_{e\in\mathcal{E}_h} \|w - \Pi^0_{0,K} w\|_e \|[\partial_{\boldsymbol{t}_e} v_h] - \Pi^0_{0,e} [\partial_{\boldsymbol{t}_e} v_h]\|_e,
\end{aligned}$$

where we have used the minimization property of $L^2$ projection and $e$ is an edge of $K$. As done in the last step of (4.21), we immediately obtain

$$E_{A2}(u, v_h) \lesssim h^{1/2}\|f\|\|v_h\|_{\varepsilon,h}.$$

For $E_{A3}(u, v_h)$, we choose $k = 2$ with the formula given in (4.12), i.e.,

$$E_{A3}(u, v_h) = \sum_{K\in\mathcal{T}_h} \varepsilon^2\big(\nabla\Delta u, \nabla(I_h^c v_h - v_h)\big)_K + (f, I_h^c v_h - v_h),$$

where

$$|(f, I_h^c v_h - v_h)| \lesssim h\|f\|\|v_h\|_{\varepsilon,h}$$

is the direct consequence of the interpolation error estimate in (3.19). We obtain from the Cauchy-Schwarz inequality, the trace inequalities (2.3) and (2.4), and the interpolation error estimates (3.17) and (3.18) that

$$\begin{aligned}
&\Big|\sum_{K\in\mathcal{T}_h}\big(\nabla\Delta u, \nabla(I_h^c v_h - v_h)\big)_K\Big| \\
=&\Big|\sum_{K\in\mathcal{T}_h}\int_{\partial K}\Delta u\frac{\partial(I_h^c v_h - v_h)}{\partial \boldsymbol{n}_e}\mathrm{d}s - \int_K \Delta u\Delta(I_h^c v_h - v_h)\mathrm{d}x\Big| \\
\le&\sum_{K\in\mathcal{T}_h}\|\Delta u\|_{0,\partial K}\Big\|\frac{\partial(I_h^c v_h - v_h)}{\partial \boldsymbol{n}_e}\Big\|_{0,\partial K} + \sum_{K\in\mathcal{T}_h}\|\Delta u\|_{0,K}|I_h^c v_h - v_h|_{2,K} \\
\lesssim&\Big(h^{1/2}\|\Delta u\|_0^{1/2}\|\Delta u\|_1^{1/2} + \|\Delta u\|_0\Big)|v_h|_{2,h}.
\end{aligned}$$

This implies

$$\varepsilon^2\Big|\sum_{K\in\mathcal{T}_h}\big(\nabla\Delta u, \nabla(I_h^c v_h - v_h)\big)_K\Big| \lesssim (h^{1/2} + \varepsilon^{1/2})\|f\|\|v_h\|_{\varepsilon,h} \lesssim h^{1/2}\|f\|\|v_h\|_{\varepsilon,h}$$

if $\varepsilon \le h$. On the other hand, for $\varepsilon \ge h$,

$$\varepsilon^2\Big|\sum_{K\in\mathcal{T}_h}\big(\nabla\Delta u, \nabla(I_h^c v_h - v_h)\big)_K\Big| \lesssim \varepsilon h|u|_3\|v_h\|_{\varepsilon,h} \lesssim h\varepsilon^{-1/2}\|f\|\|v_h\|_{\varepsilon,h} \lesssim h^{1/2}\|f\|\|v_h\|_{\varepsilon,h}.$$

Step 3: It remains to discuss the consistency terms $\varepsilon^2 J_1(I_h u, v_h)$ and $\varepsilon^2 J_3(I_h u, v_h)$. By the trace inequality, the boundedness of $\Pi_h^\nabla$, the Dupont-Scott theory, the interpolation error estimate in Lemma 4.1, and the regularity result in Lemma 4.5, we have

$$\begin{aligned}
\varepsilon^2 J_1(I_h u, v_h) &= \varepsilon^2\sum_{e\in\mathcal{E}_h}\frac{\lambda_e}{|e|}\Big\|\Big[\frac{\partial(\Pi_h^\nabla I_h u - u)}{\partial \boldsymbol{n}_e}\Big]\Big\|_{0,e}\Big\|\Big[\frac{\partial\Pi_h^\nabla v_h}{\partial \boldsymbol{n}_e}\Big]\Big\|_{0,e} \\
&\lesssim \varepsilon^2\Big(\sum_{K\in\mathcal{T}_h} h_K^{-1}\big(\|\nabla(\Pi_h^\nabla I_h u - u)\|_{0,K}^2 + \|\nabla(\Pi_h^\nabla I_h u - u)\|_{0,K}|\nabla(\Pi_h^\nabla I_h u - u)|_{1,K}\big)\Big)^{1/2} \\
&\quad\times\Big(\sum_{e\in\mathcal{E}_h}\frac{\lambda_e}{|e|}\Big\|\Big[\frac{\partial\Pi_h^\nabla v_h}{\partial \boldsymbol{n}_e}\Big]\Big\|_{0,e}^2\Big)^{1/2} \\
&\lesssim \varepsilon\Big(\sum_{K\in\mathcal{T}_h} h_K^{-1}(h_K^2|u|_{2,K}^2 + h_K^2|u|_{2,K}|u|_{3,K})\Big)^{1/2}\|v_h\|_{\varepsilon,h} \\
&\lesssim \varepsilon h^{1/2}(|u|_2 + |u|_2^{1/2}|u|_3^{1/2})\|v_h\|_{\varepsilon,h} \lesssim h^{1/2}\|f\|\|v_h\|_{\varepsilon,h}.
\end{aligned}$$

The estimation of $\varepsilon^2 J_3(I_h u, v_h)$ can be carried out similarly, so we omit the details with the result given by

$$\varepsilon^2(J_1(I_h u, v_h) + J_3(I_h u, v_h)) \lesssim h^{1/2}\|f\|\|v_h\|_{\varepsilon,h}.$$

The uniform estimate follows by combining the above bounds. □

## 5 Numerical Examples

In this section, we report the performance with several examples by testing the accuracy and the robustness with respect to the singular parameter $\varepsilon$. Unless otherwise specified, we only consider the lowest-order element ($k = 2$) and the domain $\Omega$ is taken as the unit square $(0, 1)^2$. Note that we also perform the numerical test for $k = 3$ in Example 5.2 and consider the original penalty term (3.11) in [47] in Example 5.1.

All examples are implemented in MATLAB R2019b. Our code is available from GitHub (https://github.com/Terenceyuyue/mVEM) as part of the mVEM package which contains efficient and easy-following codes for various VEMs published in the literature. The subroutine Fourth_order_Singular_Perturbation_IPVEM.m is used to compute the numerical solutions. The test script main_Fourth_order_Singular_Perturbation_IPVEM.m verifies the convergence rates.

In contrast to the jump and average terms in [47], we include the elliptic projector $\Pi_h^\nabla$ for all $v$ and $w$ in $J_i$ for $i = 1, 2, 3$. This modification simplifies the implementation process, as $\{\varphi_j = \Pi_h^\nabla \phi_j\}$ are polynomials with the same formulation, where $\{\phi_j\}$ represent the basis functions on an element. Consequently, we can assemble the integrals involving jumps and averages in a manner consistent with finite element methods. According to Lemma 3.3, we choose the penalty parameter as follows:

$$\lambda_e = \begin{cases} c_p \dfrac{N_K k(k-1)h_e^2}{4}\Big(\dfrac{1}{|T_+|} + \dfrac{1}{|T_-|}\Big), & e \in \mathcal{E}_h^0, \\ c_p \dfrac{N_K k(k-1)h_e^2}{2|T_+|}, & e \in \mathcal{E}_h^\partial, \end{cases}$$

where $c_p = 10$ is fixed in the implementation, and $|T_\pm|$ are approximated by $|K_\pm|/N_{K_\pm}$.

***Example 5.1*** The source term is chosen in such a way that the exact solution is

$$u = 10x^2y^2(1-x)^2(1-y)^2\sin(\pi x).$$

Let $u$ be the exact solution of (1.1) and $u_h$ the discrete solution of the underlying VEM (3.12). Since the VEM solution is not explicitly known inside the polygonal elements, we will evaluate the errors by comparing the exact solution $u$ with the elliptic projections. In this way, the discrete error in terms of the discrete energy norm is quantified by

$$\text{Err} = \Big(\sum_{K\in\mathcal{T}_h} (\varepsilon^2|u - \Pi_h^\Delta u_h|_{2,K}^2 + |u - \Pi_h^\nabla u_h|_{1,K}^2)\Big)^{1/2}/\|f\|. \tag{5.1}$$

To evaluate the accuracy of the proposed method, we examine a series of meshes consisting of a Centroidal Voronoi Tessellation of the unit square with 32, 64, 128, 256, and 512 polygons. These meshes are generated by using the MATLAB toolbox—PolyMesher as described in [36]. The convergence orders of the errors against the mesh size $h$ are shown in Table 1. As depicted in Table 1, the VEM guarantees at least first-order convergence for all

**Table 1** The convergence rate for Example 5.1

| $\varepsilon$ | $N$ | | | | | |
|---|---|---|---|---|---|---|
| | 32 | 64 | 128 | 256 | 512 | Rate |
| 1e−0 | 9.2232e−03 | 7.3116e−03 | 5.2637e−03 | 3.5514e−03 | 2.5748e−03 | 0.94 |
| 1e−1 | 5.5746e−02 | 3.7892e−02 | 2.5102e−02 | 1.6605e−02 | 1.1956e−02 | 1.13 |
| 1e−2 | 1.5752e−02 | 9.0565e−03 | 4.9733e−03 | 2.8939e−03 | 1.7836e−03 | 1.59 |
| 1e−3 | 1.1201e−02 | 5.9377e−03 | 3.0171e−03 | 1.5586e−03 | 7.9157e−04 | 1.92 |
| 1e−4 | 1.1151e−02 | 5.8820e−03 | 2.9494e−03 | 1.4981e−03 | 7.4851e−04 | 1.95 |
| 1e−5 | 1.1151e−02 | 5.8817e−03 | 2.9491e−03 | 1.4977e−03 | 7.4819e−04 | 1.95 |

**Table 2** The convergence rate for Example 5.1 for the IPVEM in [47]

| $\varepsilon$ | $N$ | | | | | |
|---|---|---|---|---|---|---|
| | 32 | 64 | 128 | 256 | 512 | Rate |
| 1e−0 | 9.2237e−03 | 7.3111e−03 | 5.2636e−03 | 3.5513e−03 | 2.5752e−03 | 0.94 |
| 1e−1 | 5.5755e−02 | 3.7893e−02 | 2.5104e−02 | 1.6606e−02 | 1.1958e−02 | 1.13 |
| 1e−2 | 1.5761e−02 | 9.0610e−03 | 4.9759e−03 | 2.8965e−03 | 1.7842e−03 | 1.59 |
| 1e−3 | 1.1201e−02 | 5.9379e−03 | 3.0171e−03 | 1.5592e−03 | 7.9180e−04 | 1.91 |
| 1e−4 | 1.1151e−02 | 5.8820e−03 | 2.9494e−03 | 1.4981e−03 | 7.4851e−04 | 1.95 |
| 1e−5 | 1.1151e−02 | 5.8817e−03 | 2.9491e−03 | 1.4977e−03 | 7.4819e−04 | 1.95 |

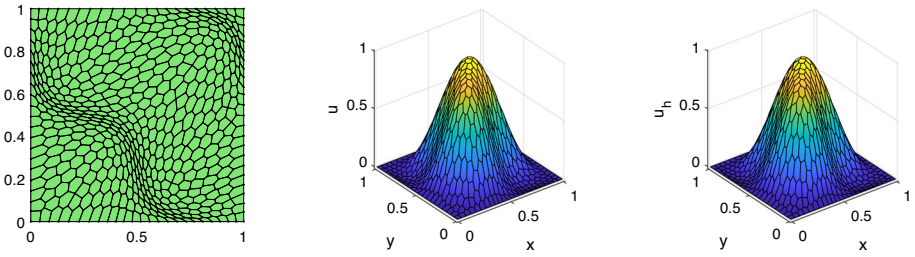


**Fig. 1** Numerical and exact solutions for Example 5.2 ($\varepsilon = 10^{-10}$)

$\varepsilon \in (0, 1]$. As $\varepsilon$ approaches zero, a nearly quadratic convergence rate is observed, aligning with the theoretical prediction in Theorem 4.1. Additionally, a stable error trend is noted in this case.

We remark that our analysis also applies to the original penalty term (3.11) in [47] when replacing $\lambda$ by $\lambda_e$ as in our approach. Using the same parameters, we conduct numerical simulations for this original form, with the results displayed in Table 2. We observe nearly identical results. The test script main_Fourth_order_Singular_Perturbation_IPVEM_Zhao.m.

***Example 5.2*** The exact solution is given by $u = \sin(\pi x)^2 \sin(\pi y)^2$.

In this example, we repeat the numerical simulation using distorted meshes illustrated in Fig. 1, showcasing both the numerical and exact solutions for $\varepsilon = 10^{-10}$. These two figures exhibit good agreement. The convergence rates of the errors relative to the mesh size $h$ are detailed in Table 3, revealing similar trends to those observed in Example 5.1.

**Table 3** The convergence rate for Example 5.2

| $\varepsilon$ | $N$ | | | | | |
|---|---|---|---|---|---|---|
| | 32 | 64 | 128 | 256 | 512 | Rate |
| 1e−0 | 1.3415e−02 | 1.1296e−02 | 8.1918e−03 | 5.7422e−03 | 3.9235e−03 | 0.90 |
| 1e−1 | 6.9122e−02 | 4.8663e−02 | 3.1364e−02 | 2.0491e−02 | 1.3783e−02 | 1.18 |
| 1e−2 | 1.7342e−02 | 9.4543e−03 | 5.3183e−03 | 2.9671e−03 | 1.7928e−03 | 1.64 |
| 1e−3 | 1.3685e−02 | 7.1795e−03 | 3.7623e−03 | 1.9493e−03 | 9.8000e−04 | 1.90 |
| 1e−4 | 1.3676e−02 | 7.1647e−03 | 3.7491e−03 | 1.9344e−03 | 9.6726e−04 | 1.91 |
| 1e−5 | 1.3676e−02 | 7.1647e−03 | 3.7491e−03 | 1.9343e−03 | 9.6720e−04 | 1.91 |

**Table 4** The convergence rate for Example 5.2 ($k = 3$)

| $\varepsilon$ | $N$ | | | | | |
|---|---|---|---|---|---|---|
| | 32 | 64 | 128 | 256 | 512 | Rate |
| 1e−0 | 3.6576e−03 | 1.1565e−03 | 4.9453e−04 | 2.0609e−04 | 9.9773e−05 | 2.58 |
| 1e−2 | 2.5411e−03 | 1.0781e−03 | 4.1860e−04 | 1.6267e−04 | 7.0703e−05 | 2.61 |
| 1e−4 | 1.8290e−03 | 5.8290e−04 | 2.0491e−04 | 6.8709e−05 | 2.3952e−05 | 3.12 |
| 1e−6 | 1.8299e−03 | 5.8332e−04 | 2.0511e−04 | 6.8796e−05 | 2.3987e−05 | 3.12 |
| 1e−8 | 1.8299e−03 | 5.8332e−04 | 2.0511e−04 | 6.8796e−05 | 2.3987e−05 | 3.12 |

Let $(\xi, \eta)$ be the coordinates on the original mesh. The nodes of the distorted mesh are obtained by the following transformation

$$x = \xi + t_c \sin(2\pi\xi)\sin(2\pi\eta), \quad y = \eta + t_c \sin(2\pi\xi)\sin(2\pi\eta),$$

where $(x, y)$ is the coordinate of new nodal points; $t_c$, taken as 0.1 in the computation, is the distortion parameter.

We also perform the numerical test for $k = 3$, with the results displayed in Table 4, frow which we observe the optimal second-order convergence when $\varepsilon$ is relatively large and third-order convergence when $\varepsilon$ tends to zero. The test script is main_Fourth_order_Singular_Perturbation_IPVEM_k3.m. Similar behaviors are observed for problems with boundary layers in the next three examples. For this reason, we opt to exclude the numerical outcomes. Interested readers can reproduce the experiments by executing our provided code.

***Example 5.3*** In this example, we test the performance of the VEM to resolve a solution with boundary layer effect. The solution with a layer is constructed such that

$$u(x, y) = \varepsilon\,(\exp(-x/\varepsilon) + \exp(-y/\varepsilon)) - x^2 y.$$

The right-hand side $f(x, y) = 2y$ is independent of the singular parameter $\varepsilon$.

We continue to examine the distorted meshes outlined in Example 5.2. The convergence rates for small $\varepsilon$ are consolidated in Table 5. Despite the presence of strong boundary layers in the exact solution, a stable trend with a quadratic convergence rate is still evident. Numerical and exact solutions are displayed in Fig. 2.

**Table 5** The convergence rate for Example 5.3

| $\varepsilon$ | $N$ | | | | | |
|---|---|---|---|---|---|---|
| | 32 | 64 | 128 | 256 | 512 | Rate |
| 1e−5 | 6.3121e−03 | 3.0943e−03 | 1.5859e−03 | 7.9631e−04 | 3.9847e−04 | 1.99 |
| 1e−6 | 6.3124e−03 | 3.0943e−03 | 1.5859e−03 | 7.9544e−04 | 3.9481e−04 | 1.99 |
| 1e−7 | 6.3125e−03 | 3.0943e−03 | 1.5860e−03 | 7.9545e−04 | 3.9482e−04 | 1.99 |
| 1e−8 | 6.3125e−03 | 3.0943e−03 | 1.5860e−03 | 7.9546e−04 | 3.9482e−04 | 1.99 |
| 1e−10 | 6.3125e−03 | 3.0943e−03 | 1.5860e−03 | 7.9546e−04 | 3.9482e−04 | 1.99 |

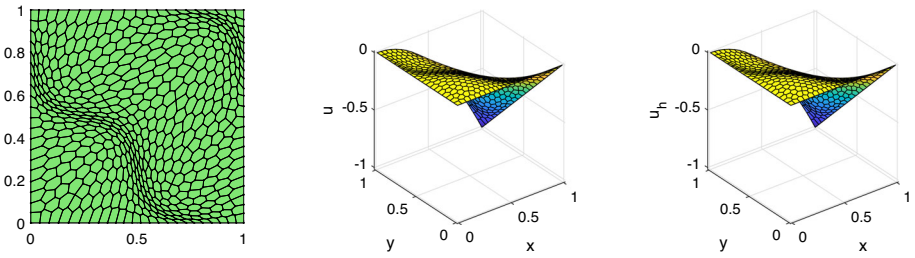


**Fig. 2** Numerical and exact solutions for Example 5.3 ($\varepsilon = 10^{-10}$)

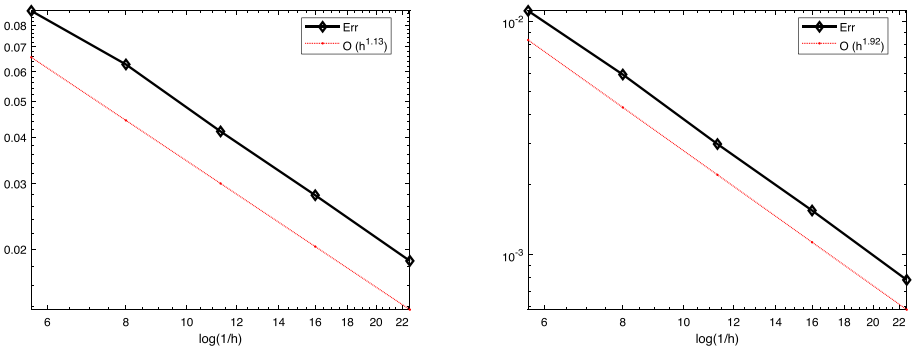


(a) $\varepsilon = 1$ (b) $\varepsilon = 10^{-10}$

**Fig. 3** The convergence rate for Example 5.4

***Example 5.4*** In this example, we once again assess the capability of the VEM to handle a solution affected by boundary layers. The exact solution takes on a more intricate form, defined as

$$u = \left(\exp(\sin \pi x) - 1 - \pi\varepsilon \frac{\cosh \frac{1}{2\varepsilon} - \cosh \frac{2x-1}{2\varepsilon}}{\sinh \frac{1}{2\varepsilon}}\right) \times \left(\exp(\sin \pi y) - 1 - \pi\varepsilon \frac{\cosh \frac{1}{2\varepsilon} - \cosh \frac{2y-1}{2\varepsilon}}{\sinh \frac{1}{2\varepsilon}}\right).$$

The convergence rates for the distorted meshes with $\varepsilon = 1$ and $\varepsilon = 10^{-10}$ are depicted in Fig. 3. Similar behaviors to those in the last example are observed. Additionally, we evaluate

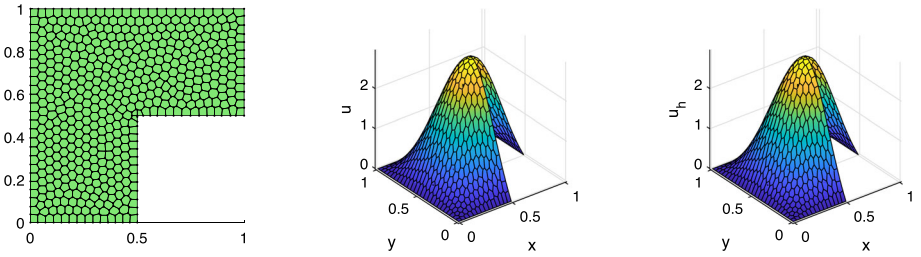


**Fig. 4** Numerical and exact solutions for Example 5.4 ($\varepsilon = 10^{-10}$)

**Table 6** The convergence rate for Example 5.4 on an L-shaped domain

| $\varepsilon$ | $N$ | | | | | |
|---|---|---|---|---|---|---|
| | 100 | 200 | 300 | 400 | 500 | Rate |
| 1e−4 | 1.7175e−03 | 8.7719e−04 | 6.5765e−04 | 6.1015e−04 | 5.8073e−04 | 1.39 |
| 1e−6 | 1.7089e−03 | 8.4014e−04 | 5.5722e−04 | 4.1990e−04 | 3.3295e−04 | 2.06 |
| 1e−8 | 1.7089e−03 | 8.4014e−04 | 5.5722e−04 | 4.1990e−04 | 3.3295e−04 | 2.06 |
| 1e−8 | 1.7089e−03 | 8.4014e−04 | 5.5722e−04 | 4.1990e−04 | 3.3295e−04 | 2.06 |
| 1e−10 | 1.7089e−03 | 8.4014e−04 | 5.5722e−04 | 4.1990e−04 | 3.3295e−04 | 2.06 |

**Table 7** The convergence rate for Example 5.5

| $\varepsilon$ | $N$ | | | | | |
|---|---|---|---|---|---|---|
| | 32 | 64 | 128 | 256 | 512 | Rate |
| 1e−6 | 8.6803e−03 | 4.3553e−03 | 2.2699e−03 | 1.1487e−03 | 5.7240e−04 | 1.95 |
| 1e−8 | 8.6803e−03 | 4.3553e−03 | 2.2699e−03 | 1.1487e−03 | 5.7240e−04 | 1.95 |
| 1e−10 | 8.6803e−03 | 4.3553e−03 | 2.2699e−03 | 1.1487e−03 | 5.7240e−04 | 1.95 |

the performance on an L-shaped domain (refer to Fig. 4 for a snapshot of the numerical and exact solutions). The meshes are composed of 100, 200, 300, 400, and 500 polygons, with the corresponding results presented in Table 6.

***Example 5.5*** For the Poisson problem (4.14), the exact solution is taken as

$$u^0(x, y) = \sin(\pi x)\sin(\pi y).$$

Then we compute the right-hand side of (1.1) by

$$f = -\Delta u^0 = 2\pi^2 \sin(\pi x)\sin(\pi y).$$

The solution $u$ of the singular perturbation problem displays strong boundary layers for very small $\varepsilon$, but the solution $u$ is unknown. So we focus on the error [34]

$$\|u^0 - u_h\|_{\varepsilon,h} \lesssim (\varepsilon^{1/2} + h^{1/2})\|f\|.$$

For very small $\varepsilon(\leq h)$, we can ensure a half-order convergence for the error $\|u^0 - u_h\|_{\varepsilon,h}$. By assessing the relative error in (5.1) with $u$ replaced by $u^0$, we consistently observe second-order convergence in this example (see Table 7).

**Acknowledgements** The authors deeply appreciate the anonymous referees for their meticulous line-by-line examination and for providing valuable comments and suggestions, which greatly improved an earlier version of the paper.

**Author Contributions** Fang Feng and Yue Yu collaborated closely to shape the conceptualization, methodology, and writing of this research. Additionally, Yue Yu took charge of implementing the discrete method in the study. Fang Feng also checked the implementation details.

**Funding** Fang Feng was supported by the National Science Foundation for Young Scientists of China (No. 12401528) and also partially supported by Central Government Special Fund for Basic Scientific Research Business Expenses of Colleges and Universities, No. 30924010837. Yue Yu was partially supported by the National Science Foundation for Young Scientists of China (No. 12301561).

**Data Availability** Data sharing is not applicable to this article as no data was generated or analyzed.

## Declarations

**Conflict of interest** The authors declare that they have no known competing financial interests or personal relationships that could have appeared to influence the work reported in this paper.

## References

1. Adak, D., Natarajan, S.: Virtual element method for semilinear sine-Gordon equation over polygonal mesh using product approximation technique. Math. Comput. Simul. **172**, 224–243 (2020)
2. Ahmad, B., Alsaedi, A., Brezzi, F., Marini, L.D., Russo, A.: Equivalent projectors for virtual element methods. Comput. Math. Appl. **66**(3), 376–391 (2013)
3. Alvarez, S.N., Beirão Da Veiga, L., Dassi, F., Gyrya, V., Manzini, G.: The virtual element method for a 2D incompressible MHD system. Math. Comput. Simul. **211**, 301–328 (2023)
4. Antonietti, P.F., Beirão da Veiga, L., Manzini, G.: The Virtual Element Method and Its Applications. Springer, Cham (2022)
5. Antonietti, P.F., Bruggi, M., Scacchi, S., Verani, M.: On the virtual element method for topology optimization on polygonal meshes: a numerical study. Comput. Math. Appl. **74**(5), 1091–1109 (2017)
6. Antonietti, P.F., Manzini, G., Verani, M.: The fully nonconforming virtual element method for biharmonic problems. Math. Models Methods Appl. Sci. **28**(2), 387–407 (2018)
7. Beirão Da Veiga, L., Brezzi, F., Cangiani, A., Manzini, G., Marini, L.D., Russo, A.: Basic principles of virtual element methods. Math. Models Methods Appl. Sci. **23**(1), 199–214 (2013)
8. Beirão Da Veiga, L., Brezzi, F., Marini, L.D., Russo, A.: The Hitchhiker's guide to the virtual element method. Math. Models Methods Appl. Sci. **24**(8), 1541–1573 (2014)
9. Beirão Da Veiga, L., Dassi, F., Manzini, G., Mascotto, L.: The virtual element method for the 3D resistive magnetohydrodynamic model. Math. Models Methods Appl. Sci. **33**(3), 643–686 (2023)
10. Beirão Da Veiga, L., Lovadina, C., Vacca, G.: Virtual elements for the Navier-Stokes problem on polygonal meshes. SIAM J. Numer. Anal. **56**(3), 1210–1242 (2018)
11. Beirão Da Veiga, L., Mora, D., Vacca, G.: The Stokes complex for virtual elements with application to Navier–Stokes flows. J. Sci. Comput. **81**, 990–1018 (2019)
12. Brenner, S.C.: Poincaré–Friedrichs inequalities for piecewise $H^1$ functions. SIAM J. Numer. Anal. **41**(1), 306–324 (2003)
13. Brenner, S.C., Neilan, M.: A $C^0$ interior penalty method for a fourth order elliptic singular perturbation problem. SIAM J. Numer. Anal. **49**, 869–892 (2011)
14. Brenner, S.C., Scott, L.R.: The Mathematical Theory of Finite Element Methods. Springer, New York (2008)
15. Brenner, S.C., Sung, L.: $C^0$ interior penalty methods for fourth order elliptic boundary value problems on polygonal domains. J. Sci. Comput. **22**(23), 83–118 (2005)
16. Brezzi, F., Buffa, A., Lipnikov, K.: Mimetic finite differences for elliptic problems. M2AN Math. Model. Numer. Anal. **43**(2), 277–295 (2009)
17. Brezzi, F., Marini, L.D.: Virtual element methods for plate bending problems. Comput. Methods Appl. Mech. Eng. **253**, 455–462 (2013)
18. Bringmann, P., Carstensen, C., Streitberger, J.: Local parameter selection in the $C^0$ interior penalty method for the biharmonic equation. J. Numer. Math. **6**, 66 (2023)

19. Cáceres, E., Gatica, G.N.: A mixed virtual element method for the pseudostress-velocity formulation of the Stokes problem. IMA J. Numer. Anal. **37**, 296–331 (2017)
20. Cangiani, A., Manzini, G., Sutton, O.J.: Conforming and nonconforming virtual element methods for elliptic problems. IMA J. Numer. Anal. **37**(3), 1317–1354 (2016)
21. Chen, L., Huang, J.: Some error analysis on virtual element methods. Calcolo **55**(1), 5 (2018)
22. Chen, L., Huang, X.: Nonconforming virtual element method for $2m$-th order partial differential equations in $R^n$. Math. Comput. **89**(324), 1711–1744 (2020)
23. Chi, H., Pereira, A., Menezes, I.F.M., Paulino, G.H.: Virtual element method (VEM)-based topology optimization: an integrated framework. Struct. Multidiscip. Optim. **62**(3), 1089–1114 (2020)
24. Chinosi, C., Marini, L.D.: Virtual element method for fourth order problems: $L^2$-estimates. Comput. Math. Appl. **72**(8), 1959–1967 (2016)
25. Ciarlet, P.G.: The Finite Element Methods for Elliptic Problems. North-Holland, Amsterdam (1978)
26. De Dios, B.A., Lipnikov, K., Manzini, G.: The nonconforming virtual element method. ESAIM Math. Model. Numer. Anal. **50**(3), 879–904 (2016)
27. Feng, F., Han, W., Huang, J.: Virtual element method for an elliptic hemivariational inequality with applications to contact mechanics. J. Sci. Comput. **81**(3), 2388–2412 (2019)
28. Feng, F., Han, W., Huang, J.: A nonconforming virtual element method for a fourth-order hemivariational inequality in Kirchhoff plate problem. J. Sci. Comput. **90**(3), 89 (2022)
29. Gatica, G.N., Munar, M.: A mixed virtual element method for the Navier–Stokes equations. Math. Models Methods Appl. Sci. **28**(14), 2719–2762 (2018)
30. Huang, J., Yu, Y.: A medius error analysis for nonconforming virtual element methods for Poisson and biharmonic equations. J. Comput. Appl. Math. **386**, 113229 (2021)
31. Ling, M., Wang, F., Han, W.: The nonconforming virtual element method for a stationary Stokes hemivariational inequality with slip boundary condition. J. Sci. Comput. **85**(3), Paper No. 56 (2020)
32. Liu, X., Li, J., Chen, Z.: A nonconforming virtual element method for the Stokes problem on general meshes. Comput. Methods Appl. Mech. Eng. **320**, 694–711 (2017)
33. Nilssen, T.K., Tai, X., Winther, R.: A robust nonconforming $H^2$-element. Math. Comput. **70**(234), 489–505 (2001)
34. Qiu, J., Wang, F., Ling, M., Zhao, J.: The interior penalty virtual element method for the fourth-order elliptic hemivariational inequality. Commun. Nonlinear Sci. Numer. Simul. **127**(4644807), Paper No. 107547 (2023)
35. Semper, B.: Conforming finite element approximations for a fourth-order singular perturbation problem. SIAM J. Numer. Anal. **29**(4), 1043–1058 (1992)
36. Talischi, C., Paulino, G.H., Pereira, A., Ivan Menezes, F.M.: Polymesher: a general-purpose mesh generator for polygonal elements written in Matlab. Struct. Multidiscip. Optim. **45**(3), 309–328 (2012)
37. Wang, F., Wei, H.: Virtual element method for simplified friction problem. Appl. Math. Lett. **85**(3820290), 125–131 (2018)
38. Wang, F., Wu, B., Han, W.: The virtual element method for general elliptic hemivariational inequalities. J. Comput. Appl. Math. 389(4194398), Paper No. 113330 (2021)
39. Wang, F., Zhao, J.: Conforming and nonconforming virtual element methods for a Kirchhoff plate contact problem. IMA J. Numer. Anal. **41**(2), 1496–1521 (2021)
40. Wang, M.: On the necessity and sufficiency of the patch test for convergence of nonconforming finite elements. SIAM J. Numer. Anal. **39**(2), 363–384 (2001)
41. Wang, M., Xu, J., Hu, Y.: Modified Morley element method for a fourth order elliptic singular perturbation problem. J. Comput. Math. **24**(2), 113–120 (2006)
42. Warburton, T., Hesthaven, J.S.: On the constants in $hp$-finite element trace inverse inequalities. Comput. Methods Appl. Mech. Eng. **192**(25), 2765–2773 (2003)
43. Xiao, W., Ling, M.: Virtual element method for a history-dependent variational–hemivariational inequality in contact problems. J. Sci. Comput. **96**(3), Paper No. 82 (2023)
44. Zhang, B., Zhao, J.: The virtual element method with interior penalty for the fourth-order singular perturbation problem. Commun. Nonlinear Sci. Numer. Simul. **133**, Paper No. 107964 (2024)
45. Zhang, B., Zhao, J., Chen, S.: The nonconforming virtual element method for fourth-order singular perturbation problem. Adv. Comput. Math. **46**(2), Paper No. 19 (2020)
46. Zhang, X., Chi, H., Paulino, G.H.: Adaptive multi-material topology optimization with hyperelastic materials under large deformations: a virtual element approach. Comput. Methods Appl. Mech. Eng. **370**(4129484), 112976 (2020)

47. Zhao, J., Mao, S., Zhang, B., Wang, F.: The interior penalty virtual element method for the biharmonic problem. Math. Comp. **92**(342), 1543–1574 (2023)
48. Zhao, J., Zhang, B., Chen, S., Mao, S.: The Morley-type virtual element for plate bending problems. J. Sci. Comput. **76**(1), 610–629 (2018)